INSTITUTE OF PHYSICS PUBLISHING MEASUREMENT SCIENCE AND TECHNOLOGY

Meas. Sci. Technol. **12** (2001) 597–614 www.iop.org/Journals/mt PII: S0957-0233(01)20350-6

Statistical frequency measuring error of the quadrature demodulation technique for noisy single-tone pulse signals

Jürgen W Czarske

Laser Zentrum Hannover eV, Hollerithallee 8, D-30419 Hannover, Germany

E-mail: cz@lzh.de

Received 2 January 2001, accepted for publication 20 February 2001

Abstract

The standard deviation of the centre frequency of a signal is investigated for the quadrature demodulation technique (QDT). Signal frequencies can be measured by QDT unaffected by the amount of available signal periods. It can be used for the measurement of nonstationary signals generated by laser Doppler velocimeters. The dependence of the frequency measuring error on the averaging time of noisy single-tone Gaussian pulse signals is analysed. Assuming a quantum noise process, it is shown that the minimum measuring error results for an averaging time of approximately $1/\mathrm{e}^2$ of the pulse duration of the signal. Alternatively, defined weighting of the measured values leads to a monotonically decreasing measuring error with increasing averaging time until the Cramer–Rao lower bound is reached. Therefore, the weighted QDT provides the lowest measuring error of all linear unbiased frequency estimators. It allows the evaluation of small frequency changes of laser Doppler signals, e.g. from micro-turbulent flows. The theory presented here is verified by Monte Carlo simulations and experiments.

Keywords: metrology, interferometry, laser Doppler velocimetry, signal processing, frequency measurement error, Cramer–Rao lower bound

1. Introduction

Frequency measurements of single-tone signals are important in several fields of research and technology. Some examples are sonar, radar and lidar, as well as communication technology, biomedicine and especially interferometric measurement techniques like laser Doppler velocimetry (LDV). The measurement of the signal frequency can be classified roughly into two principles: the time domain processing, e.g. by the zero-point-crossing counter, and the frequency domain processing, e.g. by fast Fourier transformation (FFT) [1] or the wavelet transformation [2]. Algorithms working with time–frequency distributions are used for Wigner–Ville processors [3]. Currently, the counter and FFT processors are standard devices for frequency measurements. They are usually implemented, for instance, in digital sampling oscilloscopes. However, precise frequency measurements by either method require several signal periods within an averaging time interval. This demand becomes obvious looking in the time domain: the centre frequency $\hat{f}$ can be determined, over the number n of zero points of a single-tone signal. For an averaging time t_A, the frequency is given by $\hat{f} = n/(2t_A)$. At least two zero points, i.e. one signal period, are necessary for the frequency measurement and for a high measurement accuracy, averaging over several signal periods is desired. The temporal resolution of the measurement of low frequencies is therefore limited. A similar dependence is valid for the FFT processor [4]. To overcome this drawback, the quadrature demodulation technique (QDT) was proposed [5]. In principle, the QDT allows precise frequency measurements of a pair of signals in quadrature, independently of the number of signal periods available [3–7]. Therefore, also low signal frequencies can be measured in a time-resolved way in the signal base band.

An important characteristic of a signal processing technique is the measuring error obtained. As a fundamental principle, the uncertainty relation of Heisenberg is well known. A finite signal duration implies spectral broadening, see equation (B.1) in appendix B. The ambiguity function, defined as the product of the duration of the signal and the frequency broadening, describes this relation [8]. For example, in radar technology the ambiguity function is generally used to

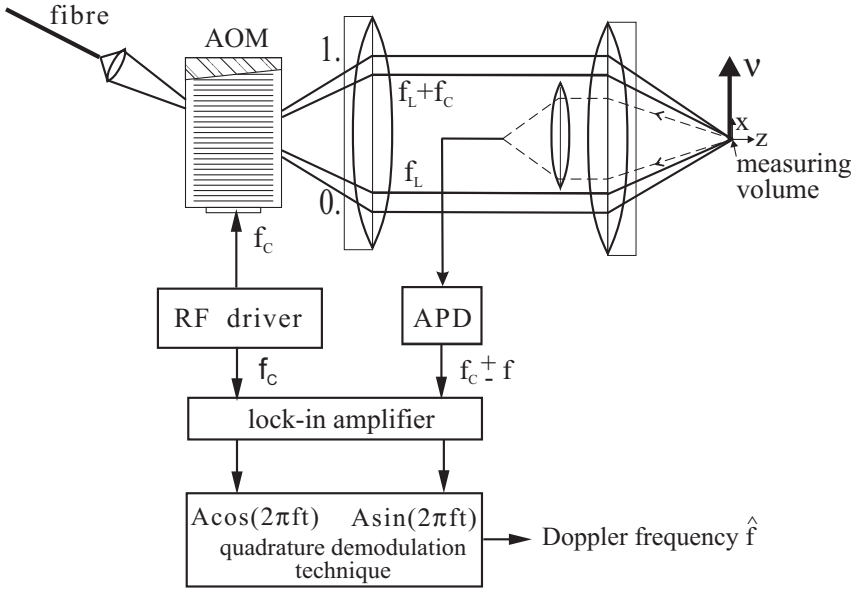

Figure 1. The principle of the quadrature demodulation technique (QDT), based on a heterodyne LDV arrangement. The light of the laser with an optical frequency f_L is split by an acoustic-optical-modulator (AOM) into the zeroth and first diffraction order [27]. A Mach–Zehnder interferometer measures the lateral velocity component along the x direction, according to $v = df$, where d is the fringe spacing in the measuring volume and f is the ideal Doppler frequency. The back-scattered light from the measuring volume is detected by an avalanche photo-diode (APD) and mixed with a reference signal from a radio-frequency (rf) driver, employing a lock-in amplifier. Measuring the phase angle $\phi_M(t) = 2\pi ft + \phi_N$ (ϕ_N: phase noise) of the generated pair of signals in quadrature yields, by means of linear regression, the estimated Doppler frequency $\hat{f} = \hat{v}/d$.

describe the reciprocity between the spatial resolution and the velocity measuring accuracy, which are proportional to the pulse duration and the resolution of the Doppler frequency [8], respectively. Besides the limitation of the signal duration, the occurring noise results in a fluctuation of the signal amplitude and thus disturbs the measurement of the signal frequency. This can be described by an uncertainty relation between the amplitude fluctuation and the phase error [9], see equation (B.2) in appendix B. Both of the fundamental signal parameters, the finite signal duration and the power of the noise process, lead to the Cramer–Rao lower bound (CRLB), which is expressed as [10]

$$(\Delta\hat{f})^2 = 3/[\pi^2\,\mathrm{SNR}\,T_s^2 N(N^2-1)] \qquad (1)$$

where the signal-to-noise ratio is defined by $\mathrm{SNR} = A^2/\sigma^2$, with A as the amplitude of the deterministic single signal and σ^2 as the variance of the white noise process; the parameter T_s is the sampling period and N is the number of sampling points of independent discrete-time observations. One presumption of equation (1) is that the signal is superposed upon an uncorrelated Gaussian noise process.

The averaging time t_A of the measurement is usually assumed to be equal to the signal duration Δt. Considering an odd number N of samples, the averaging time is given by $t_A = (N-1)T_s$. Without limiting the general validity, equation (1) can be written as

$$(\Delta\hat{f})^2 = 3/\{\pi^2\,\mathrm{SNR}\,t_A^2 N[(N+1)/(N-1)]\}. \qquad (2)$$

The CRLB describes the minimum variance of any linear unbiased frequency estimator. A signal processing procedure which in principle satisfies the CRLB is the FFT technique, whereby an interpolation among the discrete frequency spectrum values is accomplished [1, 11–17]. However, several signal periods are necessary in order to reduce the systematic frequency error sufficiently and to separate the Doppler spectral line from the level of the photo-current signal as well. If non-integer numbers of periods within the signal interval or non-symmetrical signal envelopes occur, the shape of the spectral line has furthermore a large influence on determination of the centre frequency. Restriction of the interpolation procedure to the frequency values close to the top of the spectral line can result in a measuring error greater than the CRLB. Furthermore, the use of windows, resulting in an attenuation of the amplitude at the boundaries of the signal interval, will decrease the power of the signal, so that part of the information content will be lost.

Besides the FFT technique, several other signal processing techniques have been applied to process noisy sinusoidal pulse signals [18–25]. Formerly phase-locked-loop techniques and electrical spectrum analysers were often used as frequency-domain measurement techniques, but they require stationary signals. Real LDV signals are usually pulses, which can be processed by counter and FFT processors. However, the theoretical description of the resulting frequency measuring error was carried out only rudimentarily. So, equations (1) and (2) are valid only for signals with constant amplitudes. Ruck *et al* [26] have attempted to represent pulse signals by a time-dependent SNR function. A sliding short-time SNR was calculated with an averaging time of one signal period. The Gaussian signal shape corresponds to a SNR function with an approximately Gaussian dependence. It could be set into relation with the common definition of SNR as an average value of the whole pulse signal. The measuring error of the counter technique for LDV pulse signals was investigated in terms of this concept. As a result, the existence of an optimum

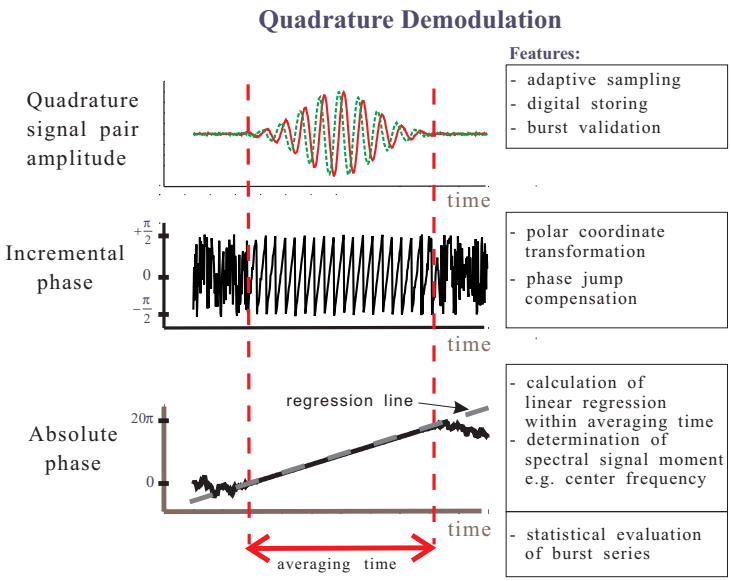

Figure 2. The evaluation of a simulated Gaussian burst signal by the QDT. The interference phase is determined from the complex pair of signals in quadrature. Incremental counting of the periods yields the absolute phase curve. The centre frequency is determined by the least squares method (LSM), considering a defined averaging time.

averaging time for Gaussian single-tone signals was shown. The minimum error of the centre frequency was obtained with the following averaging times t_A: (i) $1/\mathrm{e}$ pulse duration, for a signal-dependent noise process and (ii) $1/\sqrt{\mathrm{e}}$ pulse duration, for a signal-independent noise process [26]. Therefore, for signal processing by the counter technique, these optimal averaging times have to be taken into account.

The goal of this paper is to analyse the centre frequency measuring error of the QDT. In contrast to the FFT technique, the envelope of the signal has no influence on the measurement result. Neither is a small number of signal periods critical for processing by the QDT. This shows clearly the high potential for its use in LDV. It had already been shown [3, 4, 7, 12, 14] that the QDT reaches the CRLB. However, a detailed investigation of the measuring error for noisy single-tone pulse signals had hitherto not been presented. The particular emphasis of this paper is placed upon the examination of the optimal averaging time for the QDT system. Its advantages for processing LDV signals will be made evident by comparing its measurement characteristics with those of the counter and the FFT as representatives of standard signal processing techniques.

2. The quadrature demodulation technique

The quadrature demodulation technique (QDT) comprises the generation of a sine–cosine pair of signals, the measurement of the signal phase and its evaluation in order to determine the signal frequency. Figure 1 shows an example scheme for the generation of quadrature signals, employing a heterodyne LDV system [27]. A carrier-frequency LDV signal is electrically down-mixed with a pair of reference signals of the same carrier frequency, resulting in a background-level-free pair of signals in quadrature $a_S(t) = A(t)\sin\phi(t)$ and $a_C(t) = A(t)\cos\phi(t)$, which can be regarded as a complex phasor $a(t) = a_C(t) + \mathrm{j}a_S(t) = A(t)\exp(\mathrm{j}\phi(t))$, with $\mathrm{j}^2 = -1$. The incremental phase can be determined from $\phi(t) := \arctan(a_S(t)/a_C(t))$, with $\phi(t) = 2\pi f t$, where f is the ideal signal frequency [5]. Owing to the periodicity of the tangent function, phase jumps occur at the values $\pi/2$, $3\pi/2$, $5\pi/2$, etc., figure 2. The phase jumps of the amount π have to be detected, so that they can be added to the incremental phase curve, resulting in an unwrapped absolute phase function, figure 2. The measured phase values are fitted to a straight phase regression line

$$\hat{\phi} = \hat{a} + \hat{b}t \tag{3}$$

by means of the least-squares method (LSM) and the estimated slope $\hat{b}/(2\pi)$ gives the centre frequency $\hat{f}$ of the signal for a chosen averaging time, figure 2. The estimation procedure generally has to fulfil the following demands [28–32].

(i) Consistency. The estimate converges towards the true value of the frequency as the number of measurements, i.e. phase values, increases.

(ii) Unbiasedness. The bias is defined as the deviation of the frequency expectation value $E[\hat{f}] = \langle\hat{f}\rangle$ from the true frequency f. Although unbiasedness and consistency are related to each other, they describe different features of the estimation; e.g. an asymmetrical distribution of the estimate is biased but can nevertheless be consistent.

(iii) Efficiency. The information content I[1] of the measuring signal can be defined by the Fisher number F [8, 12, 28, 30]

$$I_a(\hat{f}) := F = \int \left(\frac{\partial \ln L(a|\hat{f})}{\partial \hat{f}}\right)^2 L(a|\hat{f})\,\mathrm{d}a$$

[1] The information content is often used in the sense of the gain in information, i.e. the difference between the information entropy, defined by Shannon, before and after a measurement. Entropy is a well-known figure of merit in communication techniques. In measuring technique it is diametrical to the signal quality, that the entropy is maximized with increasing noise power. Since the entropy is also strongly dependent on the probability density function of the measuring signal, it cannot be suitable in measuring processes, see [30].

where $L(a|\hat{f})$ is the likelihood function of the measuring signal $a(t)$ with respect to the frequency $\hat{f}$ as the estimation variable. The likelihood function describes the probability distribution of the measurement process, which is often given by a Gaussian normal function. The reciprocal of the Fisher number is equal to the variance of the MLE process, assuming that the variables of the Fisher matrix are independent. The CRLB is the variance of an efficient estimator, see equations (1) and (2). A suitable figure of merit of a signal processing technique can be defined as the quotient of the theoretical CRLB over the measuring variance obtained[2]. One estimation procedure, which is based on the maximum-likelihood estimator (MLE), is the LSM. With the Gauss–Markov rule [28] the LSM can be proved an efficient estimator, assuming that one has a Gaussian noise probability distribution. Linear regression methods shall be considered for other distribution functions [28]. For a double-exponential distribution the use of the L_1 norm instead of the L_2 norm is optimal. The norm L_p is given as the sum of the amounts to the pth degree of the deviations. In general, the optimal norm can be chosen as follows [28]. For distributions with longer tails than the Gaussian function, $p < 2$, whereas, for distributions with shorter tails, $p > 2$ is optimal. However, the L_2 norm achieves good results also for distributions other than Gaussian. Furthermore, the central limit theorem [8] states that, for a large number of measured values, the probability distribution approaches the Gaussian normal distribution. Hence, the choice of the LSM is not arbitrary, for it is a suitable algorithm for most signals.

Using the LSM for the QDT, the L_2 norm, i.e. the sum S over the squares of the differences between the measured phase values ϕ_{Mi} and the estimated phase values $\hat{\phi}_i$, has to be minimized, see appendix A:

$$S = \sum_{i=-(N-1)/2}^{i=(N-1)/2} (\phi_{Mi} - \hat{\phi}_i)^2 w_i.$$

The weighting w_i takes into account the varying error of the measured phase values. The normalized weighting is defined by

$$w_i := (\Delta\phi_{min})^2/(\Delta\phi_{Mi})^2 \tag{4}$$

where $\Delta^2\phi_{min}$ is the minimum value of the phase variance for the whole time series.

However, besides the weighted LSM, sometimes the unweighted LSM has to be chosen. (i) In general, the weight distribution is *a priori* unknown. Although the weighting is given by the signal amplitude, the noise characteristics of the photo-detector have to be known. Furthermore, noise processes like quantization noise, flicker noise and superposed laser noise can exhibit different dependences. Accurate determination of the weighting for pulse signals requires time-resolved calculation of the phase variance, which is complicated. (ii) The computer load of the weighted QDT is significantly higher than that of the unweighted QDT, see equations (A.1) and (A.2). First, the number of multiplication steps in the numerator is half that in the weighted QDT. Secondly, only one multiplication step is required for the calculation of the denominator in equation (A.2). This simplification is allowed since the sampling times can be written as $t_i = ct_i'$, where t_i' are constant values and c corresponds to the actual sampling frequency. The denominator turns out to be

$$\sum_{i=-(N-1)/2}^{i=(N-1)/2} (ct_i')^2 = c^2 \sum_{i=-(N-1)/2}^{i=(N-1)/2} t_i'^2.$$

The constant value of the sum can be used for the calculation of the denominator in equation (A.2). The *a priori* unknown weightings w_i do not allow such a simplification for the weighted QDT. In conclusion, the unweighted QDT attains a higher data rate, but a lower measurement accuracy, than the weighted QDT. Therefore, the measurement error will be investigated for both cases of the QDT.

3. The objective

As mentioned in section 1, two fundamental parameters influence the frequency measuring error: the signal duration Δt and the SNR. However, for the observation of an nonstationary signal like a pulse, neither parameter can be defined easily. The SNR of a pulse has to be described by a time-dependent function, see [26]. The resulting time-dependent variance of the measured phase implies that the measuring for the error centre frequency depends on the averaging time t_A. Let this be outlined by two examples.

(i) The averaging time t_A is much less than the signal duration Δt. A short averaging time corresponds to a small number of measured values. The information content of the signal will be evaluated incompletely, so that a high measuring error will result. This is also evident from the occurrence of a broad-banded Fourier spectrum for a short signal interval, compare with equation (B.1).

(ii) The averaging time t_A is much greater than the signal duration Δt. The continuous decrease of the SNR in the remote tail regions of the pulse signal, i.e. for a high signal time, causes noisy measured values. Employing these measured values in the frequency determination may also result in a large measuring error.

In consequence, the optimum averaging time can be expected to lie in between these two boundary conditions. One main objective of this paper is to determine this supposed optimum averaging time for the QDT.

4. Theoretical investigations

4.1. The model and approach

Let us assume that we have a real sinusoidal signal pulse with a Gaussian amplitude envelope $A(t) = A_0 \exp[-(t/\tau)^2]$. Upon this ideal signal there is superposed an additive noise process $n(t)$, resulting in the measurement signal

$$a_M(t) = A_0 \exp(-(t/\tau)^2) \sin(\omega t) + n(t) \tag{5}$$

[2] Assuming that one has a biased estimation process, a lower variance than the CRLB can be achieved. If it is possible to find an estimate of the bias of such an estimator, its result can be corrected and an unbiased estimator with reduced variance is achieved. However, reliable processing of such a reduced variance unbiased estimator is difficult to accomplish for experimental signals.

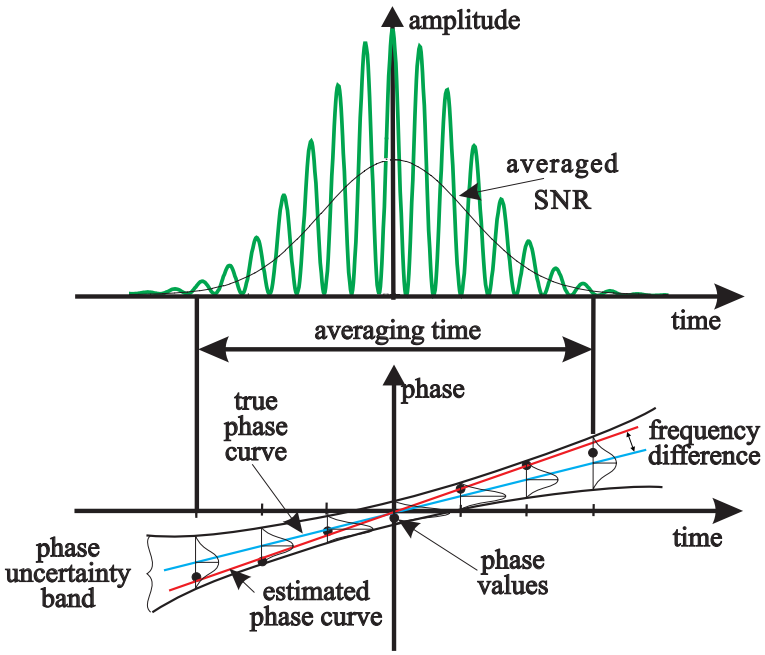

Figure 3. A model of frequency measurement with a QDT system. The noisy phase samples exhibit a deviation from the ideal (true) phase curve of a single-tone signal. The difference between the angles of the estimated phase regression curve and the ideal phase curve yields the frequency measuring error.

where A_0 is the maximum signal amplitude, τ is the $1/\mathrm{e}$ half duration of the signal and $\omega = 2\pi f$ is the ideal circle frequency. The duration Δt of the signal is generally set to the $1/\mathrm{e}^2$ full duration $\Delta t = \tau 2\sqrt{2}$. To simplify the description, only one part of the complex quadrature signal, see section 2, is considered.

Figure 3 shows the signal model for the investigation of the QDT processor. The ideal (noise-free) signal is described by the phase $\phi = 2\pi f t$, see equation (5). Owing to the noise process $\phi_N(t)$ the measuring phase values $\phi_{Mi} = \phi_i + \phi_{Ni}$, $i = -(N-1)/2, \ldots + (N-1)/2$ are disturbed and lie inside an uncertainty band. Assuming that one has a Gaussian distribution, the confidence interval displayed in figure 3, with a width of about $\pm 3\Delta\phi$, contains 99.7% of the noisy phase samples ϕ_{Mi}. From the measured phase values an averaged phase curve $\hat{\phi} = 2\pi \hat{f} t$ is calculated by linear regression, compare with equation (3) for $\hat{a} = 0$. In general there is a difference between the estimated frequency $\hat{f}$ and the true value f. Repetition of the measurement will result in a probability density function of the frequency $\hat{f}$, figure 4. Owing to the unbiasedness of the LSM procedure, the centre frequency $\langle \hat{f} \rangle$ of the distribution is assumed to be equal to the true frequency f. Taking the standard deviation of the ensemble results in $\Delta \hat{f} = [\langle (\hat{f} - f)^2 \rangle]^{1/2}$.

As shown in figure 5, the measuring error is influenced by several signal and processor parameters. Their discussion will be carried out in sections 4.5, 5 and 6.

4.2. Signal and noise processes

The measurement signal is generated by LDV system with a lateral intensity distribution $I(x, y)$ in the centre of the measurement volume of $I(x, y) = I_0 \exp[-(x^2+y^2)/w^2][1 + v \sin(2\pi x/d)]$, where I_0 is the maximum intensity, x and

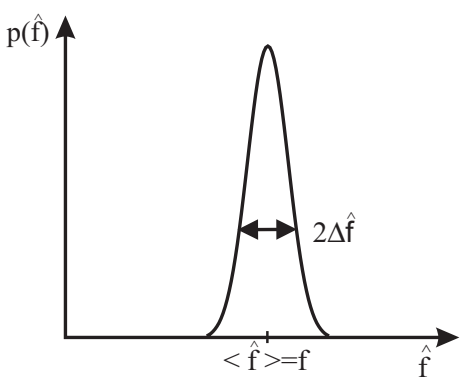

Figure 4. The probability density function of the estimated frequency of a noisy single-tone pulse signal.

y are the lateral coordinates, w is the $1/\mathrm{e}$ half width, v is the visibility of the fringe pattern and d is its spacing [25]. The measurement volume is given by the cross section of two coherent Gaussian laser beams. The infinite integral of the intensity distribution gives $\iint I(x, y)\,\mathrm{d}x\,\mathrm{d}y = I_0 \pi w^2 = P_L$, where P_L is the available laser power in the measurement volume. A single tracer particle is assumed, the diameter of which is small relative to the radius w, crossing the measurement volume with a constant velocity v in the x direction. The power of the scattered light follows as $P(t) = P_0 \exp[-(t/\tau)^2][1 + m \sin(2\pi v t/d)]$, where the correspondences between the spatial and the time domain, $x = vt$ and $w = v\tau$, are used. The scattered light generates a photo-current signal, according to $A = Pq\eta/(h\upsilon) = kP$, where η is the quantum efficiency, h is Planck's quantum, υ is the optical frequency and $k = q\eta/(h\upsilon)$ is a proportionality constant. Using only the modulated current, equation (5) results. Its parameters can be set in relation to the optical

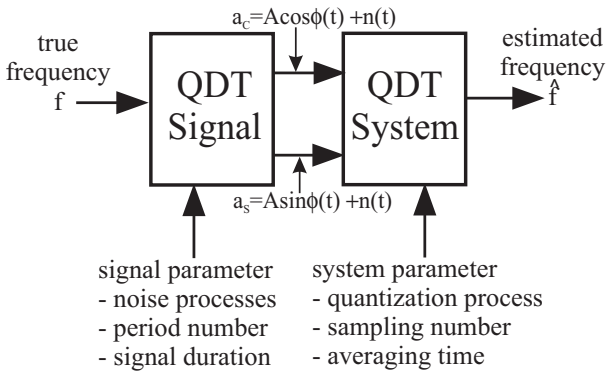

Figure 5. The scheme used for the investigation of the centre frequency error. Various key parameters of the signal and system are considered. The ideal signal phase $\phi(t) = 2\pi f t$ is disturbed by the phase noise process $\phi_N(t)$. In principle, the measuring error of the estimated frequency $\hat{f}$ is influenced by several signal parameters as well as by parameters of the QDT system. The frequency deviation results as the difference between the estimated frequency $\hat{f}$ and the true (ideal) frequency f. Evaluating the signal ensemble results in the standard deviation $\Delta\hat{f}$ of the centre frequency.

constraints of the LDV system, as follows [32]. (i) The signal amplitude $A_0 \simeq I_0 \simeq P_L/w^2$ is directly proportional to the laser power and inversely proportional to the square of the lateral size w of the measurement volume. (ii) The pulse signal duration $\Delta t = 2\sqrt{2}\tau$ is determined for example for a constant tracer particle velocity of $v = 1\ \mathrm{m\ s^{-1}}$ and a $1/\mathrm{e}^2$ lateral diameter of the measurement volume of typically $\Delta x = 2\sqrt{2}w = 100\ \mu\mathrm{m}$. Together with $\tau = w/v$, the $1/\mathrm{e}^2$ full signal duration of $\Delta t = 2\sqrt{2}\tau = 100\ \mu\mathrm{s}$ results. (iii) The ideal signal frequency is described by $f = v/d$. A typical frequency of $f = 100$ kHz results for a velocity of $v = 1\ \mathrm{m\ s^{-1}}$ and a fringe spacing of $d = 10\ \mu\mathrm{m}$. (iv) The noise process $n(t)$ is described by its variance σ^2, which depends on the elongation $a(t)$ of the signal. To simplify the description, averaging over a single period is carried out. Therefore, the variance can be regarded in terms of its dependence on the signal amplitude $A(t)$.

The intrinsic noise of a photo-detector is the shot noise, i.e. quantum noise, caused by random fluctuation of the electron current. In terms of Poisson statistics its variance turns out to be [8]

$$\sigma_S^2 = 2qA'B = c_1 A/m \tag{6}$$

where $q = 1.6 \times 10^{-19}$ A s is the electron charge, $A' = A/m$ is the directional photo-current, A is the amplitude of the bias-free sinusoidal signal, m is the modulation coefficient, B is the electrical bandwidth and c_1 is an introduced proportionality constant. The excess noise of the internal amplification process of the detector is also a shot noise process, which occurs in avalanche photo-diodes and photo-multipliers. Besides these intrinsic noise processes, the dark current of a photo-detector also causes shot noise, but it is independent of the signal amplitude and usually has a lower level.

An extrinsic noise process is the thermal noise, which is caused by the Brownian motion of the electrons. The variance results in [8]

$$\sigma_T^2 = 4kTB/R = c_2 \tag{7}$$

where k is the Boltzmann constant, T is the environmental temperature, B is the electrical bandwidth and R is the real part of the impedance of the photo-detector (c_2 is an introduced constant). Amplifiers, mixers and other electronic components also generate thermal noise. After pre-amplification of the photo-current, the signal level is significantly increased, so that the additional thermal noise is usually negligible. Of course, laser power fluctuations and other technical sources also produce noise. However, those are not of fundamental character and will therefore not be considered.

The digital processing of the photo-signal causes quantization noise. The quantized signal can be considered as the continuous function plus quantization noise, which represents the difference between the quantized values and the original continuous values. Assuming an amplitude quantization with equidistant levels, the standard deviation turns out to be $\sigma_Q = \Delta a = \Delta m/\sqrt{12}$ [33], where Δm is the quantization resolution. It is equal to $\Delta m = 2A_0/(2^b - 1)$, with b the bit number of the quantization levels. The full dynamic range of an analogue-to-digital converter (ADC) is assumed to be equal to twice the maximum amplitude $A(t = 0) = A_0$, so that no signal clipping occurs. The equivalent SNR for a sinusoidal signal is then given by [33]

$$\sigma_Q^2 = A_0^2/(3(2^b - 1)^2) = c_3 \tag{8}$$

with c_3 as an introduced constant.

In conclusion, three fundamental noise processes of the LDV signal are considered. Shot noise is an intrinsic process, caused by the quantized current of photo-detectors, see equation (6). Thermal noise in the photo-detector and the amplifiers also has to be considered, see equation (7). It can be reduced by cooling, but carrier fluctuations caused by temperature cannot be suppressed completely. Another fundamental type of noise is caused by the signal quantization due to the digital signal processing technique, see equation (8). The resulting SNR of the sinusoidal signal can be summarized as

$$\begin{aligned}\mathrm{SNR} = P_S/P_N = a_{eff}^2/\sigma^2 &= (A^2(t)/2)/(c_1 A(t)/m + c_2 + c_3) \\ &= (k^2 P^2(t)/2)/(kc_1 P(t)/m + c_2 + c_3)\end{aligned} \tag{9}$$

where the optical–electrical relation $A = kP$, the effective amplitude $a_{eff}(t) = A(t)/\sqrt{2}$ and the resulting power $\sigma^2 = \sigma_S^2 + \sigma_T^2 + \sigma_Q^2$ of the uncorrelated noise processes are used.

The asymptotes of equation (9) are given by

$$\begin{aligned}\lim(A \to 0)\,\mathrm{SNR} &= A^2(t)/(2c_2 + 2c_3) \sim A^2(t) \\ \lim(A \to \infty)\,\mathrm{SNR} &= mA(t)/(2c_1) \sim A(t).\end{aligned} \tag{10}$$

Thermal and quantization noise processes dominate at small amplitudes, whereas shot noise is prevalent at large amplitudes, i.e. SNR. However, when one is optimizing the photo-detection unit by employing an avalanche diode, a transimpedance pre-amplifier and a high-resolution ADC, the shot noise regime can also be reached for a moderate SNR.

The phase noise can be derived by error propagation [34] as well as by statistical interpretation of the noise distribution of a complex phasor [32]. The standard deviation yields

$$\Delta\phi_M = (2 \cdot \mathrm{SNR})^{-1/2} \qquad \mathrm{SNR} \gg 1. \tag{11}$$

The experimental determination of the signal phase exhibits a demodulation threshold of SNR $\cong$ 9 dB $\cong$ 8 [4, 14].

Therefore equation (11) is considered valid for a SNR > 9 dB. However, with implementation of a modified phase evaluation, correcting parasitary counts of noise-induced periods (clicks), the demodulation threshold can be reduced to lower than 5 dB.

In summary, the standard deviation of the signal phase according to equations (5), (10) and (11) is given by the following.

(i) For a signal-dependent noise process, i.e. shot noise (regime 1),

$$\Delta\phi_M(t) \sim \mathrm{SNR}^{-1/2}(t) \sim A^{-1/2}(t) \sim \exp[(t/\tau)^2/2]. \quad (12)$$

(ii) For a signal-independent noise process, i.e. thermal noise (regime 2α) and quantization noise (regime 2β),

$$\Delta\phi_M(t) \sim \mathrm{SNR}^{-1/2}(t) \sim A^{-1}(t) \sim \exp[(t/\tau)^2]. \quad (13)$$

The relations developed assume a dependence of the SNR on the envelope $A(t)$ of the sinusoidal signal. As shown in section 2, a complex signal $a(t) = a_C(t) + \mathrm{j}a_S(t)$ is processed by the QDT. In comparison with equation (9) the complex SNR results in: $\mathrm{SNR} = \langle a_S^2(t) + a_C^2(t)\rangle/[\sigma_S^2(t) + \sigma_C^2(t)] = A^2(t)/[2\sigma^2(t)]$, where the Pythagorean angle rule $a_S^2(t) + a_C^2(t) = A^2(t)[\sin^2\phi(t) + \cos^2\phi(t)] = A^2(t)$ and the equality of the uncorrelated noise processes $\sigma_S^2(t) = \sigma_C^2(t) = \sigma^2(t)$ are used. The assumed cross correlation function relating the noise processes of the sine and cosine signals of zero is valid for independent noise sources. In principle the complex signal can physically be generated both by the homodyne and by the heterodyne LDV technique [5]. Separated noise processes are given for the homodyne technique, using two photo-detectors for the generation of the sine and cosine signals [32]. Regarding thermal and quantization noise processes, their variances are independent of the signal, which results in the proportionality $\mathrm{SNR} \propto A^2(t)$, see equations (10) and (13). For shot noise the variance depends on the elongation of the signal $a(t)$, but integration over one signal period [26] allows as an approximation the same description as that shown above. Therefore, equations (10) and (12) describe the shot noise by invoking the assumed proportionality $\sigma^2(t) \propto A(t)$. In the case of the heterodyne technique the shot noise and the thermal noise generated in the same photo-detector, figure 1, are correlated. Averaging of the variance of the noise over one signal period can also simplify their description. As an approximation the SNR results in the formulae given above.

Finally, the probability density function of the phase noise is considered. Thermal noise has a Gaussian distribution, which can be shown by the central limit theorem [8]. A large number of elementary current pulses occur, having a time scale of the order of the interval between inter-electron collisions, which is around 10^{-14} s at room temperature. Since the duration of these elementary events is significantly smaller than the typical signal duration of about $\Delta t = 100\ \mu$s (see above), stationarity and ergodicity of the noise process can be presupposed. For shot noise a Poisson distribution results, which can be approximated by a Gaussian distribution for higher numbers of events. In contrast to these noise processes of the analogue signal, quantization noise is described by a uniform distribution [33]. Furthermore, the quantization effect can be treated as a noise process only if an arbitrary sampling of a high number of available quantization levels occurs. Otherwise, in the case of only a few quantization levels, deterministic effects will happen. Section 5.1 deals with these characteristics.

The phase noise of a pair of signals in quadrature, formulated in polar coordinates, can be considered on the basis of amplitude noise [29]. The assumed Gaussian noise processes of the signal amplitudes exhibit a Rayleigh amplitude distribution in polar coordinates, with a uniform phase noise distribution in $[0, 2\pi[$. The measuring signal is defined as the sum of an ideal signal and this Rayleigh noise distribution, which leads to a Rice distribution [29]. The phase noise distribution becomes $p(\phi_M) = \exp(-\mathrm{SNR}\sin^2\phi_M)\sqrt{\mathrm{SNR}}\cos\phi_A/\sqrt{\pi}$, $\mathrm{SNR} > 1$. Assuming that $\mathrm{SNR} \gg 1$, the Rice phase distribution can be approximated by a Gaussian distribution. In conclusion, a white Gaussian phase noise process of the pair of signals in quadrature results.

4.3. Assumptions

In this section, the parameters of the LDV signal are considered. The assumptions for the investigation of the measuring error are summarized as follows.

(i) We have a single-tone sinusoidal signal, equation (5). Scattering from a single moving tracer particle in the measurement volume is considered. Multiple-scattering processes are neglected.

(ii) We have a Gaussian function of the signal amplitude, equation (5). The fundamental-mode laser beams employed generate a Gaussian shape of the intensities in the measurement volume. Regarding straight motion of a particle with constant velocity v in the x direction, figure 1, a sinusoidal signal of constant frequency f with a Gaussian signal envelope results. Deviations from the Gaussian shape can be obtained if asymmetrically orientated receiving optics with beam stops are employed. Since the QDT algorithm is robust against different signal envelopes it has not to be considered.

(iii) We have a Gaussian distribution of the phase noise, section 4.2. It was shown that the Gaussian probability density function is a good approximation for a $\mathrm{SNR} \gg 1$. Since the LSM applied is robust against differences in noise distributions [28, 35], the uniform distribution of the quantization noise will be ignored in the investigations.

(iv) We have a white phase noise, i.e. statistically independent phase values, section 4.2. Shot and thermal noise can be described as white noise processes. Usually the noise bandwidth is significantly broader than the linewidth of the Doppler signal spectrum. The sampling frequency is assumed to be twice the signal frequency and smaller than the noise bandwidth. Then phase values that are assumed to be uncorrelated result. However, in real signal processing, the sampling theorem of Shannon [33] also applies to the noise signal. Partial correlation of the measured values has to be considered for these investigations.

(v) We have deterministic sampling times. Usually quartz clocks are applied. They have a low jitter for such short time durations of $\Delta t = 100\ \mu$s as are typical for LDV

signals, see section 4.2. Also their long-term drift of about 1 s per year (3×10^{-8}) is sufficiently low. The sampling time jitter corresponds to the clock jitter, since precision of sample-and-hold circuits can be assumed in comparison with the typical relative phase error of $\Delta\phi/(2\pi) \approx 10^{-2}$ for a signal with a SNR of 20 dB, the sampling jitter can be neglected. This allows the assumption of a one-dimensional error distribution of the noisy phase values with deterministic sampling times, figure 3.

4.4. Results

In appendix A the measuring error of the centre frequency is derived on the basis of the assumptions in section 4.3, see also [35, 36]. Equations (A.6) and (A.7) are reformulated with the weighting function equation (4), which results, using equations (12) and (13), in

$$w_i = \exp[-m(t_i/\tau)^2] \propto A^m(t_i) \tag{14}$$

with $m = 1$ for signal dependent noise processes (regime 1) and $m = 2$ for signal-independent noise processes (regime 2). Both the unweighted and the weighted QDT are discussed. Owing to the symmetry of the Gaussian shaped signal, half of the time series with the sampling times t_i, $i = 1, \ldots, (N-1)/2$, is considered. The standard deviation of the unweighted QDT (case A) is given by

$$\Delta\hat{f} = \frac{\Delta\phi_{min}(\sum_{i=1}^{(N-1)/2} i^2 \exp[m(i/\tau)^2])^{1/2}}{(2^{3/2}\pi t_A/(N-1)) \sum_{i=1}^{(N-1)/2} i^2} \tag{15}$$

whereas, for the weighted QDT (case B),

$$\Delta\hat{f} = \frac{\Delta\phi_{min}}{(2^{3/2}\pi t_A/(N-1))(\sum_{i=1}^{(N-1)/2} i^2 \exp[-m(i/\tau)^2])^{1/2}}. \tag{16}$$

In either formula, $\Delta\phi_{min}$ is the minimum standard deviation of the time series, t_A is the averaging time, N is the number of phase samples, τ denotes the $1/\mathrm{e}$ half pulse duration and the parameter m is given as $m = 1$ for signal-dependent noise and as $m = 2$ for signal-independent noise.

4.5. Concluding remarks

4.5.1. The dependence on the averaging time. In section 3 the existence of an optimal averaging time was expected. To simplify the discussion, the result, equations (15) and (16), will be written as analogous functions. Then, the sums can be formulated as integrals. For case A,

$$\Delta\hat{f} \sim \frac{(\int_{t=0}^{t_A/2} t^2 \exp[m(t/\tau)^2]\,\mathrm{d}t)^{1/2}}{\int_{t=0}^{t_A/2} t^2\,\mathrm{d}t}$$

$$= \left[\left(\int_{t=0}^{t_A/2} t^2\{1 + m(t/\tau)^2 + [m(t/\tau)^2]^2/2 + [m(t/\tau)^2]^3/6 + \cdots\}\,\mathrm{d}t\right)^{1/2}\right][t_A^3/24]^{-1}$$

and for case B,

$$\Delta\hat{f} \sim \left(\int_{t=0}^{t_A/2} t^2\{1 + m(t/\tau)^2 + [m(t/\tau)^2]^2/2 + [m(t/\tau)^2]^3/6 + \cdots\}\,\mathrm{d}t\right)^{-1/2}. \tag{17}$$

The Gaussian function is expressed as a polynomial, since its integral cannot be solved in a closed form for finite limits. The measuring error is discussed for two examples.

(i) A short averaging time. For $\lim t_A \to 0$, only the zeroth order of the polynomial in equation (17) has to be considered. Thus the same asymptote results for both cases A and B: $\Delta\hat{f} \sim t_A^{-3/2}$. A high measuring error results, as had already been predicted in section 3.

(ii) A long averaging time. For $\lim t_A \to \infty$ the higher orders of the polynomial function have to be included in the calculation. A higher degree of the numerator than of the denominator results. Therefore, in case A the measuring error has a divergent characteristic. A high measuring error results. On the other hand, in case B a convergent dependence is obtained. The measuring error is minimized by increasing the averaging time. To summarize, the arguments mentioned in section 3 are confirmed only for case A. Case B has a different dependence for a high averaging time. This discrepancy will be investigated in section 5.

4.5.2. Continuous signals. The measuring error for a signal with a constant amplitude $A(t) = A_0$ is discussed in order to compare the result with equation (2), in section 1. Since the weighting is identical to unity, the same standard deviation of the centre frequency results for both cases (A and B):

$$\Delta\hat{f} = \frac{\Delta\phi_{min}}{(2^{3/2}t_A\pi/(N-1))(\sum_{i=1}^{(N-1)/2} i^2)^{1/2}}$$

$$\text{with } \frac{(2\sum i^2)^{1/2}}{N-1} = \left(\frac{N}{12}\,\frac{N+1}{N-1}\right)^{1/2}$$

$$\Delta\hat{f} = \frac{\sqrt{1.5}}{t_A\pi[\mathrm{SNR} \cdot N(N+1)/(N-1)]^{1/2}} \tag{18}$$

where statistically independent measurement values and a $\mathrm{SNR} = a_{eff}^2/\sigma^2 \gg 1$ of a single signal are assumed; see equation (11). Taking into account the complex pair of signals in quadrature, the same expression as that in equation (2), i.e. the CRLB, is obtained. This proves that the QDT system meets the CRLB, i.e. it is an efficient frequency estimator (section 2).

Equation (18) shall be considered in relation to the Heisenberg uncertainty relation (see appendix B).

(i) The proportionality $\Delta\hat{f} \propto t_A^{-1}$ corresponds to equation (B.1). Large averaging times for a signal with constant amplitude reduce the measuring error. However, nonstationary signals like pulses from LDV systems have a limited signal duration, see above.

(ii) The proportionality $\Delta\hat{f} \propto \mathrm{SNR}^{-1/2}$, $\mathrm{SNR} \gg 1$, corresponds to equation (B.2). A high signal quality, i.e. SNR, reduces the measuring error. However, real signals have a limited SNR, since the photo-detector current attains saturation and digital signal processing causes quantization noise.

(iii) The proportionality $\Delta\hat{f} \propto N^{-1/2}$, $N \gg 1$ corresponds to Poisson statistics, see appendix B. The number N of samples denotes the repetition of independent measurements. An increase in N reduces the measuring error until adjacent noisy phase values are correlated, see (iv) in section 4.3. Then, the available information content

of the signal is completely evaluated. The resulting measuring error will be considered for this demand. The maximum sampling frequency $f_S = 1/T_s$ is chosen to be equal to the noise bandwidth B of the signal ($f_S = B$). With equation (A4) the number of phase values turns out to be $N_{max} \cong t_A f_S = t_A B$. The SNR can be written according to section 4.2 as $\mathrm{SNR} = P_S/(p_N B)$, where P_S is the signal power and $P_N = p_N B$ is the noise power, with p_N as the spectral power density. Using these dependences, equation (18) can be written for $\mathrm{SNR} \gg 1$, $N \gg 1$ and a constant noise bandwidth B as

$$\Delta\hat{f} \sim t_A^{-1}\mathrm{SNR}^{-1/2}N_{max}^{-1/2} \sim t_A^{-1}\mathrm{SNR}^{-1/2} \sim p_N^{1/2}t_A^{-1}P_S^{-1/2}. \tag{19}$$

In conclusion, the minimum measuring error is independent of the number N_{max} of samples, when they are chosen in correspondence to the noise bandwidth. Only the fundamental signal parameters t_A and SNR determine the measuring error. This represents the Heisenberg uncertainty relation (appendix B, see also [9, 37]).

Equation (19) shall be considered in relation to the signal energy $E = P_S t_A$, assuming an equivalence of the signal duration Δt and averaging time t_A. Using the proportionality of the signal amplitude $A = P_S^{1/2}$ to SNR from equations (10), (12) and (13), the measuring error turns out to be $\Delta\hat{f} \sim t_A^{-1}A^{-1/2} \sim t_A^{-1/2}E^{-1/2}$, regime 1 and $\Delta\hat{f} \sim t_A^{-1}A^{-1} \sim E^{-1}$, regime 2. Considering regime 2, the measuring error can be directly expressed in terms of the signal energy.

4.5.3. Systematic measuring error. The resulting frequency measuring error can be divided into a statistical and a systematic error. A reduction of the statistical error can be achieved by repeating the measurements. In contrast, the systematic error forms a bias, which cannot be reduced in this way, but allows a correction of the measuring result, if it is known.

The occurring period number n of the signal interval has a strong influence on the frequency bias of the FFT technique [1, 4, 13, 17]. Since the bias is influenced by several parameters of the signal, especially the actual frequency, which has to be measured, it usually cannot be corrected. Therefore, a bias-free characteristic is important for the signal processing technique used. One major advantage of the QDT is its unbiased frequency measurement, which is principally independent of the signal's envelope function and the available number of signal periods [3–7]. A limit of the measurement performance results, however, from the quantization bit number. Using e.g. 8-bit digitization of the signals, frequency measurements can be accomplished for a period number of about 1/100 [4]. Furthermore, it has to remarked that the QDT is based on a pair of signals in quadrature, which ideally has the same amplitude, exactly 90° phase difference and no offset [5, 32]. In order to guarantee an unbiased frequency measurement, see figure 4, these presumptions have to be fulfilled. Then, the QDT ensures that bias-free frequency measurements are obtained even for a small fraction of one signal period.

4.5.4. The correspondence to the optical signal generation. The intensity distribution in the measurement volume of the LDV system will be included in the investigations of the measuring error. Equations (18) and (19) describe the absolute statistical frequency error, which can be reformulated by including the signal generation of a LDV system, see section 4.2: $f = v/d$ and $t_A = \Delta t = \Delta x/v$, where v is the velocity of the tracer particles, Δx is the lateral $1/\mathrm{e}^2$ diameter of the intensity distribution in the measurement volume and d is the spacing of the fringe pattern. The $1/\mathrm{e}^2$ full signal duration Δt is set to the averaging time t_A. Assuming a constant number N_{max} of samples, the measuring error turns out to be $\Delta\hat{f} \sim v\Delta x^{-1}\mathrm{SNR}^{-1/2}$. The accuracy is therefore reduced for high velocities. Precision measurements of supersonic flows require high SNR values, i.e. high powers of the scattered light.

The appreciation of the quality of measurement is usually accomplished by referring the absolute measurement error to the measured value. This relative measuring error is given by $\Delta\hat{f}/\hat{f} \sim t_A^{-1}\mathrm{SNR}^{-1/2}f^{-1} \sim \Delta x^{-1}\mathrm{SNR}^{-1/2}d$. According to equation (10) the SNR is expressed in terms of the signal amplitude A, which, on the other hand, is given by $A \sim I \sim P_L/(\Delta x)^2$, where I is the intensity within the measurement volume and P_L is the laser power, see section 4.2. It results in $\mathrm{SNR} \sim A^m \sim P_L^m(\Delta x)^{-2m}$, with $m = 1$ for shot noise (regime 1) and $m = 2$ for thermal and quantization noise (regime 2). The relative measurement error is given by

$$\Delta\hat{f}/\hat{f} \sim (\Delta x)^{m-1}P_L^{-m/2}d. \tag{20}$$

The relative measuring error can be minimized by increasing the laser power P_L and decreasing the fringe spacing d. A discussion of the diameter Δx of the measurement volume requires consideration of the different noise regimes. (i) For $m = 1$ there is no dependence on the size of the measurement volume. (ii) For $m = 2$, $\Delta\hat{f}/\hat{f} \sim \Delta x$, a small measurement volume has to be generated in order to minimize the relative measuring error.

Additionally, the fluid mechanics has to be considered for the dimensioning of the measurement volume. A small size is desired in order to resolve spatial changes of the velocity or to allow measurements near walls [2, 25]. However, the number n of fringes, i.e. signal periods, is then also reduced. Ongoing systematic frequency error can be reduced with the QDT, in comparison with to the usually applied FFT technique, see above.

Finally the shape of the intensity distribution is investigated. For the weighted QDT, see equations (A.3), (16) and (17), the measuring error can be considered to be

$$\Delta\hat{f} \sim \left(\int_{t=0}^{t_A/2} t^2 w(t)\,\mathrm{d}t\right)^{-1/2}$$

where $w(t)$ is a continuous weighting function, which is directly proportional to the intensity distribution I, assuming that we are in regime 1, see above. According to equation (14) it can be written as $w(t) = \exp[-m(t/\tau)^2]$. A diametrical mutual dependence of $w(t)$ and t^2 can be recognized. It can be referred to as a functional mismatching, meaning that a high quality of the signal, i.e. large values of $w(t)$, around the centre of the signal has a negligible effect on the calculated centre frequency. At the tails of the signal, where high values

of the parabolic function t^2 are available, only small values of $w(t)$ occur. In conclusion, the available power of the light source is not used for the frequency measurement in an optimal way.

A reduction of the measuring error can be achieved by matching of the functions $w(t)$ and t^2. One can generate a fringe pattern with an intensity envelope, corresponding to two laser spots having maximum values at the boundaries of the measurement volume. Then, the corresponding weighting function is matched to the parabolic function coming from the signal processing algorithm. In [30] a similar result was derived, but with a different method. However, the possible improvement of the frequency measurement is relatively small [7], so that the Gaussian intensity distribution of common LDV systems is no remarkable disadvantage.

5. Simulation results

In section 4 the measuring error of the centre frequency was theoretically derived in terms of its dependence on the averaging time of the signal. Now, a Monte Carlo computer simulation is applied. First the parameters of the signal generation and the sampling regimes are presented. A signal duration of $\Delta t = 2^{3/2}\tau = 100\ \mu$s and a period of duration $T = 10\ \mu$s are assumed. Two different sampling regimes are considered: (i) a constant sampling frequency f_S and (ii) a constant number N of measurements within the averaging time. Usually regime (i) is applied in the LDV technique, but, when a limited memory of the signal processing technique is relevant, regime (ii) has to be used. The maximum number of measurements for the simulation is set to $N_{max} = 1025$ for an averaging time of $t_A = 2\Delta t = 200\ \mu$s. Using the relation $t_i = iT_s$ for the sampling points, with $-(N-1)/2 < i < +(N-1)/2$, a constant period of $T_s = t_A/(N-1) = 200\ \mu$s$/1024 = 195$ ns results for regime (i). In contrast, regime (ii) has a sampled period of variable duration, given by $T_s = t_A/(N-1) = t_A/1024$.

According to equation (5), deterministic quadrature signals with superposed uncorrelated Gaussian white noise processes are generated. The auto-correlation functions of the simulated noise processes were proved to be equal to $\delta(n)$ each ($\delta(n)$ is the Kronecker delta).

The investigation of the measuring error is accomplished according to figure 3: A noisy Gaussian single-tone pair of signals, equation (5), having a controlled SNR, is generated and measured by a QDT system, implemented with LabVIEW on a PC. The estimated frequency is compared with the true frequency of the generated signal. After a repetition of this procedure, the measuring error is given by

$$\Delta\hat{f} = \left(\frac{1}{M'}\sum_{\mu=1}^{M}(\hat{f}_\mu - \langle\hat{f}_\mu\rangle)^2\right)^{1/2}. \qquad (21)$$

The values $\hat{f}_\mu$ are the estimated frequencies of each simulated signal, whereas $\langle\hat{f}_\mu\rangle$ is the arithmetic mean of the ensemble of signals, which is equal to the true frequency f. Since the true frequency is known for a simulation calculation, the value M' in the denominator is set to the number of measurements performed: $M' = M = 50$.

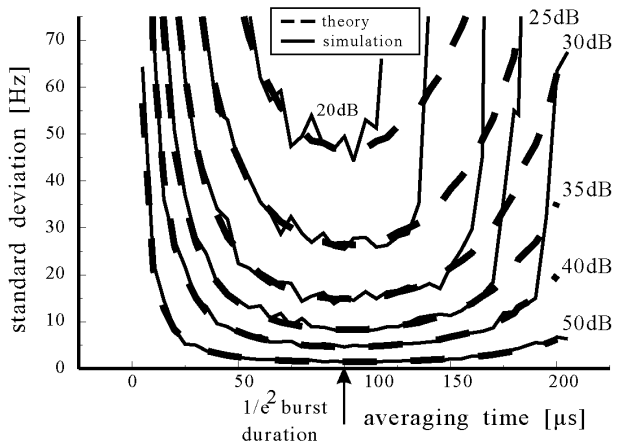

Figure 6. The statistical frequency measuring error versus the averaging time, for unweighted QDT (case A), with a shot noise process (regime 1) and constant sampling frequency (regime (i)).

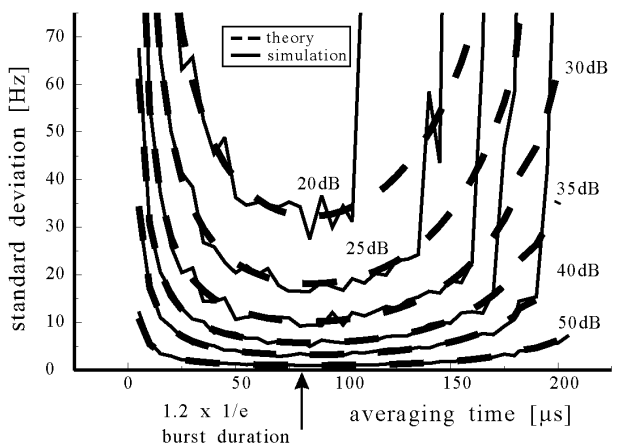

Figure 7. The statistical frequency measuring error versus the averaging time, for unweighted QDT (case A), with a shot noise process (regime 1) and constant sampling number (regime (ii)).

A simplified scientific notation for the standard deviation is used, neglecting the ensemble of signals. The derivation as an ensemble value will have to be considered in a further investigation. So the ergodicity of the noise process, i.e. the equality of the time average and ensemble average, has to be assumed. This is valid, since the time constant of the elementary noise events and the sampling period are several orders of magnitude smaller than the signal duration, see section 4.3.

5.1. Investigations on the unweighted QDT (case A)

In figures 6–11, the measuring error of the unweighted QDT is shown in terms of the dependence on the averaging time. Theoretical curves, calculated with equation (15) and Monte Carlo simulations for six different regimes resulting from the combinations of the sampling regimes (i) and (ii) and the noise regimes (1, 2α and 2β) are displayed. The SNR in each figure is defined for the maximum signal amplitude $A(t=0) = A_0$ and written as logarithmic values $\mathrm{SNR}_{dB}(t=0)$.

The minimal measuring error is achieved for defined averaging times, shown in table 1. It has to be recognized

Table 1. The optimal averaging time for a centre frequency determination by a weighted QDT (case A), determined by equation (15). Various noise processes (regimes 1 and 2) and sampling regimes (i) and (ii) for the noisy sinusoidal signal with a Gaussian pulse shape are considered. The half averaging time $t_A/2$ is compared with the $1/\mathrm{e}$ half pulse duration τ. For comparison, the results of the counter technique are shown, see [26].

	Constant sampling frequency, regime (i)	Constant number of samples, regime (ii)	Zero-point crossing counter technique
Signal-dependent noise process, regime (1)	$1.018\sqrt{2}\tau$	$0.849\sqrt{2}\tau$	τ
Signal-independent noise process, regime (2)	1.018τ	0.849τ	$1/\sqrt{2}\tau$

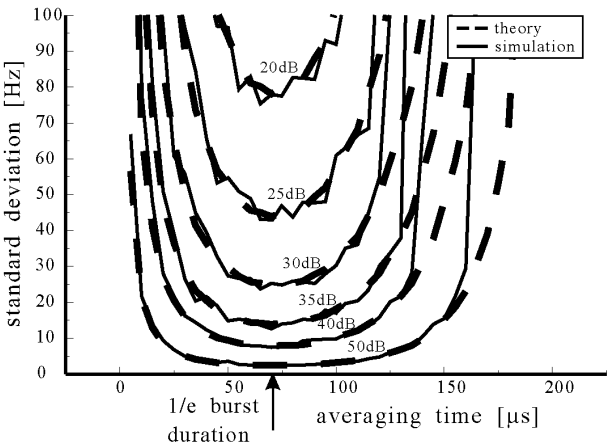

Figure 8. The statistical frequency measuring error versus the averaging time, for unweighted QDT (case A), with a thermal noise process (regime 2α) and constant sampling frequency (regime (i)).

that the optimal averaging times are independent of the SNR, see figures 6–11. However, for large SNRs also a low measuring error is obtained in the immediate vicinity of the optimal averaging times. In consequence, the tolerances of the averaging times for obtaining precise frequency measurements are enlarged.

The quotient of the optimal averaging times for the regimes 1 and 2 is exactly $\sqrt{2}$; see table 1. It is valid for both sampling regimes (i) and (ii) and also for the counter technique. This can be explained as follows. The standard deviation $\Delta\phi_M$ of the phase values is dependent on the weighting function, equation (14): $\Delta\phi_M \sim \sqrt{w} \sim \exp[-(t/\tau)^2 m/2]$, with $m = 1$ for regime 1 and $m = 2$ for regime 2. The half $1/\mathrm{e}$ duration of these distribution is $\tau(2/m)^{1/2}$. It yields $\sqrt{2}\tau$ for regime 1 and τ for regime 2, resulting in a quotient of $\sqrt{2}$.

For the different sampling regimes (i) and (ii), the optimal averaging times shall be discussed. For an averaging time of $t_A = 2\Delta t = 200$ μs, by definition the same number of samples $N_{max} = 1025$ occurs for both regimes. The standard deviations of regimes (i) and (ii) are equal (figure 6–11). For an averaging time t_A less than $2\Delta t$ the number N of samples is reduced according to $N = 1025\ t_A/(2\Delta t)$ for regime (i), but remains constant ($N = N_{max}$) for regime (ii), see above. The higher number of measurements of regime (ii) for $t_A < 2\Delta t$ results in a smaller measuring error, compare figures 6, 8 and 10 with figures 7, 9 and 11. In regime (i), the number of samples increases with the averaging time. At increasing averaging times, a stronger decrease of the measuring error results, so that the optimal averaging time of regime (i) is larger than that of regime (ii). The quotient of the optimal averaging times of the regimes (i) and (ii) is $q \approx 1.1987$, see table 1.

The counter technique can also be considered as a phase measurement procedure, but with a different sampling regime. The counter measures the zero crossing points, which occur at phase values of $0, \pi, 2\pi, 3\pi$, etc., giving a phase resolution of 1 bit per period. In contrast to the QDT, the counter determines the time points for these defined phase values. This completely different sampling regime implies other optimal averaging times than those for the QDT, see table 1.

5.1.1. Discussion of figures 6–9 (regimes 1 and 2α). The results of the theory and the simulation agree very well for small averaging times. Only a small fluctuation of the simulation curve around the theoretical curves occurs, which is caused by deviations of the SNRs for the simulated signal. The simulation results can be further improved by using a higher number M of measurements, equation (21). However, a significant discrepancy between theory and simulation occurs at great averaging times. The reason is the demodulation threshold of the phase measurement, which occurs at a SNR of 9 dB, see equation (11). In the theory this threshold was not taken into account, so that a deviation from the simulation curve results. Regarding e.g. the regime 1, the time-dependent SNR is given by $\mathrm{SNR}(t) \sim \exp[-(t/\tau)^2]$, see equation (12). Its logarithmic value $\mathrm{SNR}_{dB} = 10\log(\mathrm{SNR})$ turns out to be

$$\mathrm{SNR}_{dB} = \mathrm{SNR}_{dB}(t = 0) - 4.34(t/\tau)^2. \qquad (22)$$

The demodulation threshold is reached at a signal time $t_D = -\tau \ln(10^{-a})$, with $a = (\mathrm{SNR}_{dB}(t = 0) - 9\ \mathrm{dB})/10$ and τ as half the $1/\mathrm{e}$ signal duration. Two arbitrarily chosen values $\mathrm{SNR}_{dB}(t = 0) = 20$ and 30 dB correspond to the signal times of $t_D = 112$ and 155 μs for reaching the threshold. Since a phase measurement from these signal times is not possible, it dominates the resulting measuring error. Therefore the signal time and averaging time can be set equal as an approximation. Figures 6 and 7 show that there is a strong increase of the measuring error at these averaging times.

5.1.2. Discussion of figures 10 and 11 (regime 2β). The quantization of the signal amplitude was considered in section 4.2 as a signal-independent noise process. So the same optimal averaging times as for thermal noise (regime 2α) are obtained, see table 1. Equivalent SNR_{dB} values can be defined according to equation (8) for the quantization noise:

$$\begin{aligned}\mathrm{SNR}_{dB} &= 10\log[\mathrm{SNR}] \\ &= 10\log\{1.5(2^b - 1)^2 \exp[-2(t/\tau)^2]\} \\ &\cong 6b + 1.8 - 8.69(t/\tau)^2 \end{aligned} \qquad (23)$$

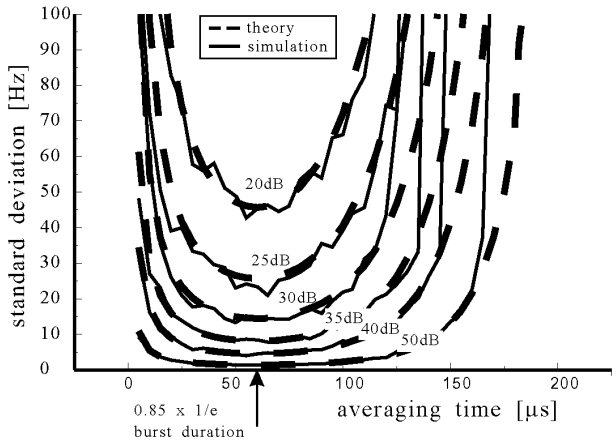

Figure 9. The statistical frequency measuring error versus the averaging time, for unweighted QDT (case A), with a thermal noise process (regime 2α) and constant sampling number (regime (ii)).

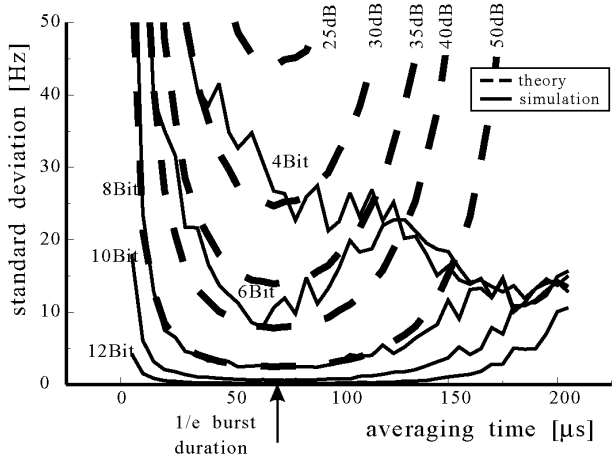

Figure 10. The statistical frequency measuring error versus the averaging time, for unweighted QDT (case A), with a quantization noise process (regime 2β) and constant sampling frequency (regime (i)).

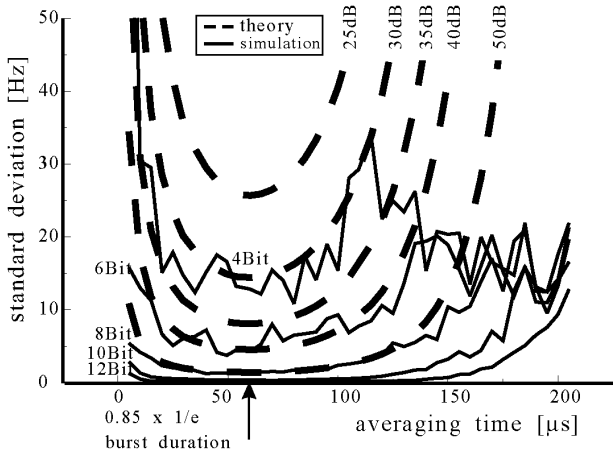

Figure 11. The statistical frequency measuring error versus the averaging time, for unweighted QDT (case A), with a quantization noise process (regime 2β) and constant sampling number (regime (ii)).

where b is the number of bits and the time-dependent signal power $A^2(t) = A_0^2 \exp[-2(t/\tau)^2]$ giving

$$\mathrm{SNR} = \frac{a_{eff}^2}{\sigma_Q^2} = \frac{A^2(t)}{2\sigma_Q^2}$$

(see equation (8)) is used.

In figures 10 and 11 simulation curves for some numbers of bits are shown. The corresponding equivalent SNRs are $\mathrm{SNR}_{dB}(4\ \mathrm{bit}) = 25.8$ dB, $\mathrm{SNR}_{dB}(6\ \mathrm{bit}) = 37.8$ dB, $\mathrm{SNR}_{dB}(8\ \mathrm{bit}) = 49.8$ dB, $\mathrm{SNR}_{dB}(10\ \mathrm{bit}) = 61.8$ dB and $\mathrm{SNR}_{dB}(12\ \mathrm{bit}) = 73.8$ dB. The theoretical curves in figure 10 and 11 have the same SNRs as those used in figures 6–9 in order to compare the quantization noise with the thermal and shot noise.

At small averaging times and high numbers of bits, a good agreement with the theory results (see the curve of $b = 8$ bit, i.e. SNR $\approx$ 50 dB). The otherwise occurring discrepancy can be explained as follows. At a low number of bits, no fluctuation of the quantization levels for adjacent sampling points takes place. Therefore, the phase values are free of quantization noise. A quantization resolution of 2 bits shall be considered. Around $b = 2$ bits only a few quantization values occur, so that the quantized phase is given by a curve with low noise. With increasing signal time the number of bits b is reduced according to equation (23) by $\Delta b = -1.44(t/\tau)^2$. For other numbers of bits $b(t = 0)$ in figures 10 and 11 a reduction to e.g. $b = 2$ bits occurs at the following signal times t: for $b = 4$ bits, $t = 83\ \mu$s, for $b = 6$ bits, $t = 118\ \mu$s, for $b = 8$ bits, $t = 144\ \mu$s for $b = 10$ bits, $t = 166\ \mu$s and $b = 12$ bits, $t = 186\ \mu$s. Beyond these signal times the quantization cannot be described as a noise process. Therefore, the simulated curves for these averaging times differ from those predicted by the theory of quantization noise. For example, for 8 bits the simulation deviates from the theoretical curve (SNR $\approx$ 50 dB) at the above-determined averaging time of 144 μs; see figures 10 and 11. A further increase of the averaging time results in a reduction of the number of bits until $b = 0$. The result for high averaging times is that the various simulation curves converge towards a smaller statistical error than do the theoretical curves corresponding to the CRLB.

However, on the other hand, the systematic error of the centre frequency is greater for long averaging times. Unbiased frequency measurements also at the tails of pulse signals require a high number of bits for the ADC. Considering a typical LDV signal, with a $\mathrm{SNR}_{dB}(t = 0)$ of 20 dB, the usually obtained resolution of 8 bits is sufficient, compare figures 6 and 8 with 10.

5.2. Investigations of the weighted QDT (case B)

The weighted QDT is analysed in terms of the dependence on the averaging time. As described in section 2, to achieve efficient frequency measurements, a heteroscedastic signal has to be weighted, see equation (4). The investigations are accomplished for two regimes (1, i) and (2α, i) with $\mathrm{SNR}(t = 0) = 30$ dB, see figures 12 and 13. It was shown in section 4.5 that the QDT achieves the CRLB of a signal, so that the theoretical curves have the minimum measuring error. Different weighting functions are used for the

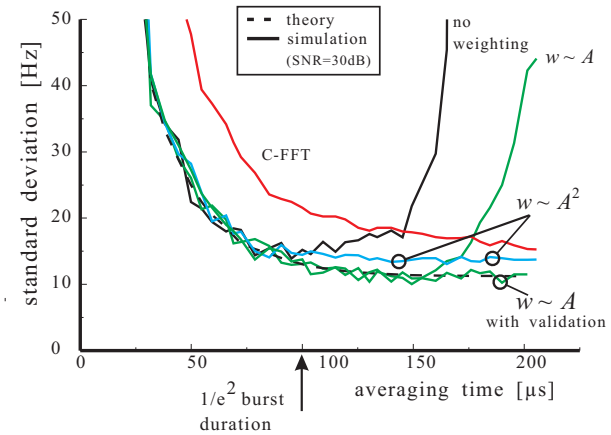

Figure 12. The statistical frequency measuring error versus the averaging time, for weighted QDT (case B), with a shot noise process (regime 1) and constant sampling frequency (regime (i)). Several weighting functions for the phase were used. For comparison, the result of a complex FFT technique with a Hanning window and seven-point arithmetic mean interpolation is shown.

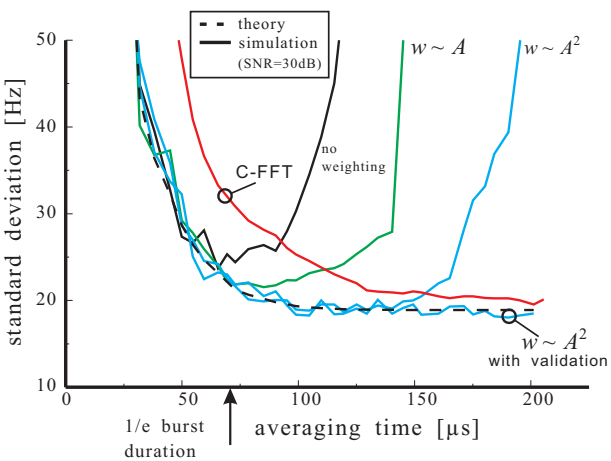

Figure 13. The statistical frequency measuring error versus the averaging time, for weighted QDT (case B), with a thermal noise process (regime 2α) and constant sampling frequency (regime (i)). Several weighting functions for the phase were used. For comparison, the result of a complex FFT technique with a Hanning window and seven-point arithmetic mean interpolation is shown.

simulation in order to attain the optimal weighting suggested by equation (14). In regimes 1 and 2 the weightings $w(t) \sim A(t)$ and $w(t) \sim A^2(t)$, respectively, have to be used. As shown in figures 12 and 13, the CRLB is exactly reached with these weighting functions. At great averaging times beyond 155 μs (see section 5.1), the signal drops below the demodulation threshold, resulting in the discrepancy between theory and simulation shown; see figure 12.

The weighting according to equation (4) is defined by the variance of the phase values. Equation (14) uses the proportionality between the phase variance and signal amplitudes. It is valid beyond the demodulation threshold of SNR $>$ 9 dB. Otherwise a weighting function with validation is used; it is set to $w \equiv 0$ for SNR $<$ 9 dB, see figures 12 and 13.

Besides results from the weighted QDT, simulation results of the unweighted QDT (see section 5.1) and the complex FFT

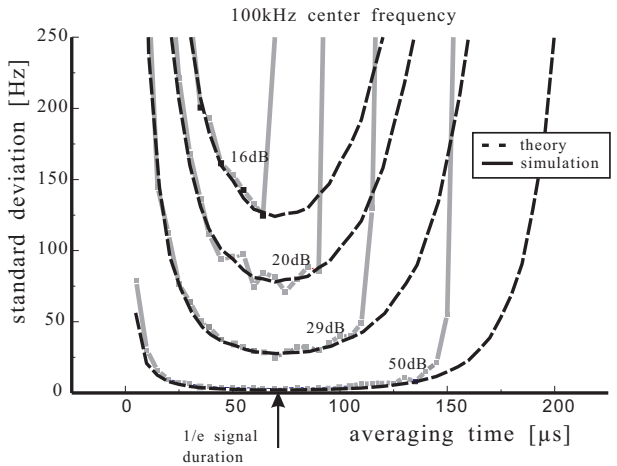

Figure 14. The statistical frequency measuring error versus the averaging time. The signal is generated with an arbitrary signal generator; for unweighted QDT (case A), with a thermal noise process (regime 2α) and constant sampling frequency (regime (i)).

technique are also shown. As can be seen from figures 12 and 13 the same dependence of the measuring error on the averaging time results for the weighted QDT and the complex FFT technique. The FFT has in reality no demodulation threshold, but the measuring error is slightly greater than the CRLB. It is mainly caused by deviations at the interpolation of the discrete frequency spectrum values for low period numbers [4, 13]. Since the number of periods in the centre of the signal is small, a significant increase of the measurement error at small averaging times occurs, see figures 12 and 13.

6. Experimental verification

In addition to the computer simulation, an experimental proof of the theory is acquired. To simplify the investigations, the unweighted QDT is used only with the thermal noise regime 2α and a sampling of constant frequency (regime i). In figure 8 the simulation curve for case A, regime 2α, (i) was shown. A verification of this result is accomplished by using first a signal generator and secondly an experimental LDV system. These two investigations were carried out with the same signal processing system, using a two-channel 8-bit PC-based data acquisition card with maximum 1024 sampling points per channel. The difference to $N_{max} = 1025$ of the simulation can be neglected. The QDT system has been implemented by means of the software LabVIEW on a PC (personal computer). The use of the signal generator includes the acquisition of data for the examination of errors, but allows the generation of signals with known parameters. Therefore, it is a suitable extension from the numerical simulation. A final verification is achieved by the LDV system, although controlling the signal parameters is more difficult.

(i) An arbitrary signal generator (LeCroy LW 420) was used to synthesize the signals. Two uncorrelated Gaussian random processes are generated and superposed on the deterministic pair of signals in quadrature. The frequency error has been calculated in the same way as described in section 5, see equation (21). Repetitions of measurements with $M = 50$ were carried out. In figure 14 the measuring

errors obtained for various values of $\mathrm{SNR}_{dB}(t = 0)$ are shown. It can be concluded from figure 14 that there is an excellent agreement of theory and measurement in the range above the demodulation threshold. The optimal averaging time is approximately given by the $1/\mathrm{e}$ signal duration, see table 1 for regime 2, (i). Quantization effects of the arbitrary generator, having 11-bit resolution, as well as from the PC data acquisition card, having 8-bit resolution, cannot be detected in the measurement result.

(ii) A heterodyne LDV system, see figure 1, is used to generate the measurement signal. A measurement volume with a full $1/\mathrm{e}^2$ diameter of $\Delta x = 2^{3/2}w = 340\ \mu$m and a spacing of $d = 10\ \mu$m of the fringe system has been generated. In order to obtain a defined measurement signal, a scattering wire was moved by a chopper through the measurement volume with a velocity of about $v = 3.4\ \mathrm{m\ s^{-1}}$. The signal generated has a duration of about $\Delta t = 2^{3/2}\tau = 100\ \mu$s and a frequency of approximately $f = 340$ kHz. Owing to the PIN photo-diode used, the thermal noise process dominates. By evaluation of the FFT spectrum, $\mathrm{SNR}_{dB}(t = 0)$ was estimated to be approximately 20 dB. The measuring error of the centre frequency was determined by means of equation (21), using $M' = M - 1 = 49$ in the denominator, since the expectation value is unknown in principle for experimental data.

The optimal averaging time is determined as approximately the $1/\mathrm{e}$ signal duration, figure 15. Hence, the theoretical result for regime 2, (i) is experimentally proved, see table 1. However, a significantly higher relative frequency error of $\Delta\hat{f}/\hat{f} \approx 2.25$ kHz/340 kHz $\approx 0.7\%$ occurs, in comparison with the theoretical result of $\Delta\hat{f}/\hat{f} \approx 80$ Hz/340 kHz $\approx 0.02\%$, see figure 8. It may be caused by disturbances in the generated signals arising from laser power fluctuations, drift of the chopper circle velocity and instabilities of the used scattering wire. Furthermore, estimation of the arrival time of the burst signal [2] and the signal envelope have to be considered. A simplified QDT algorithm, assuming a symmetrical Gaussian signal has been used; compare with equation (15), figure 2. The asymmetrical signal generated requires an adaptive definition of the evaluation time interval in order to reduce the measuring error.

7. Discussion

The standard deviations of case A, and case B of the QDT are compared. According to equation (17) the quotient of the measuring errors are given by

$$\begin{aligned}\Delta\hat{f}_{case\ A}/\Delta\hat{f}_{case\ B} &= \left[\left(\sum_{i=1}^{(N-1)/2} i^2 \exp[m(i/\tau)^2]\right)^{1/2}\right. \\ &\quad \left.\times\left(\sum_{i=1}^{(N-1)/2} i^2 \exp[-m(i/\tau)^2]\right)^{1/2}\right]\left[\sum_{i=1}^{(N-1)/2} i^2\right]^{-1} \\ &\sim \left[\left(\int_{t=0}^{t_A/2} t^2 \exp[m(t/\tau)^2]\,\mathrm{d}t\right)^{1/2}\right. \\ &\quad \left.\times\left(\int_{t=0}^{t_A/2} t^2 \exp[-m(t/\tau)^2]\,\mathrm{d}t\right)^{1/2}\right]\left[\int_{t=0}^{t_A/2} t^2\,\mathrm{d}t\right]^{-1} \quad (24)\end{aligned}$$

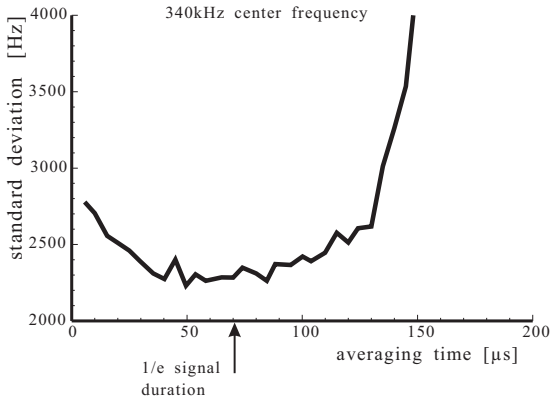

Figure 15. The statistical frequency measuring error versus the averaging time. The signal is generated by means of a heterodyne laser Doppler velocimeter; for unweighted QDT (case A), with a thermal noise process (regime 2α) and constant sampling frequency (regime (i)).

where continuous functions of the weighting are used, with $m = 1$ and $m = 2$ for the regimes 1 and 2, respectively. Premising the regime 1, the minimum measuring error of case A is obtained at an averaging time of $t_{opt} = 1.018\tau 2\sqrt{2}$, i.e. approximately the $1/\mathrm{e}^2$ signal duration, see table 1. In contrast, case B results in a minimum measuring error, which asymptotically approaches the CRLB for $t_A \to \infty$, see figures 12 and 13. Using the optimal averaging times, a quotient of $\Delta\hat{f}_{case\ A}/\Delta\hat{f}_{case\ B} = 1.3302$ results for the two cases A and B. The measuring error of case A is about 33% higher than that of case B, which is equal to the CRLB. About 67% of the square root of the information content of the signal is therefore used.

However, due to the occurring demodulation threshold, the available averaging time is practically limited. Using the averaging time t_{opt} of case A also for case B, the measuring error of case A is only 16% higher than that of case B. Then the measuring error of case B is about 15% above the CRLB. These results are valid for regime 1 as well as for regime 2 of the noise processes.

The information content of the signal, resulting in the CRLB (see section 2), is exploited by the weighted QDT. In contrast, the unweighted QDT also incorporates the noisy phase values from the tails of the signal into the determination of the centre frequency (section 4.5). According to equation (17), these uncertain phase values greatly affect the measurement result, since they are multiplied by the square of the signal time in the calculation of the centre frequency. The increase of the measuring error in comparison with case B is therefore elucidated and this answers the questions in section 3.

An optimal averaging time also results from using the counter technique, see table 1. However, a significantly higher measuring error can be observed. Assuming a signal with a constant amplitude, the standard deviation can be written as $\Delta\hat{f}_{Counter} = (\pi t_A\,\mathrm{SNR}^{1/2})^{-1}$ [26], where the averaging time t_A and the signal frequency $\hat{f}$ correspond to the zero point number n: $t_A\hat{f} = 2n$, see section 1. The quotient of the measuring error of the counter technique and the CRLB, equation (18), can be expressed as $\Delta\hat{f}_{Counter}/\Delta\hat{f}_{CRLB} \cong (N/1.5)^{1/2}$, where N is the number of uncorrelated measured values. For example, a typical number $N = 512$ of

measurement values yields a quotient of 18.5. However, it is strongly dependent on the noise bandwidth B of the signal (section 4.5).

As shown in figures 12 and 13, the measuring error of the FFT technique and the weighted QDT decrease monotonically with increasing averaging time. The uncertainty of the measuring value in the tails of the signal also increases the noise density of the FFT spectrum, but the impact on the spectral line of the Doppler signal can be neglected. Therefore, the evaluation of the signal in the frequency domain is not susceptible to the noise disturbances at small signal amplitudes. However, at very low SNRs beyond 0 dB, the noise floor can exceed the spectral line and result in a demodulation threshold of the frequency measurement. In the LDV signal processing this does not occur, because only signals with SNR > 0 dB can be triggered in the time domain. The reductions in quality of the signal due to signal clipping and quantization have a minor effect on the measuring error of the FFT technique. This has been taken advantage of in 1-bit FFT frequency measurement techniques [38].

The weighted QDT has similar characteristics to the FFT technique (figures 12 and 13). The influence of uncertain measurement values is reduced by the weighting factor, see section 5.2. However, two differences between QDT and FFT have to be pointed out. (i) The weighting has to be calculated. Therefore, the measuring error of the QDT is also dependent on the accuracy of the weighting function. (ii) The phase values exhibit a demodulation threshold, which cannot be reduced by weighting. Therefore, the QDT requires a signal of high quality, but then the CRLB can be reached exactly.

The features of the various signal processing techniques can be summarized as follows. (i) Time domain characteristics, resulting in e.g. the counter technique and unweighted QDT, can be realized with little technical effort and achieve a high data rate. However, a signal of high quality is necessary and definite averaging times have to be used in order to achieve a high measuring accuracy. (ii) With frequency domain characteristics, resulting in e.g. FFT and weighted QDT, in principle, the CRLB is asymptotically reached with great averaging times. However, the computer load is higher than that for time domain processors. As shown in figures 12 and 13 the weighted QDT exhibits the lowest measuring error of all the signal processing techniques discussed. Furthermore, the measuring error is in principle independent of the occurring period number. These advantages of the QDT are relevant for signals with a high SNR (>9 dB). Fields of application are e.g. flow LDV measurement of micro-turbulence with small eddies, sound-wave-caused accelerations [3], droplet accelerations [14], vortices after nozzles [15] and small velocities in biomedical flows. However, besides the evaluation of a single signal, the random occurrence of the signals has to be taken into account [39]. The random passages of the tracer particles through the measurement volume result in velocity samples of the flow, which are irregularly spaced in time. At low tracer particle rates, the measurement of velocity fluctuations is not free of bias due to aliasing in the sampling process. Therefore suitable estimators for the processing of LDV signal series have to be used, see [2, 40].

8. Conclusions

The quadrature demodulation technique (QDT) is presented as a precise frequency measuring procedure for single-tone signals, with inherently high SNR. The main advantages of the QDT are the independence of the frequency determination from the occurring signal period number and the shape of the signal envelope. For instance, precise frequency measurements of burst signals having only a fraction of one period can be accomplished. In this work, for the first time, a rigorous investigation of the frequency measuring error for noisy pulsed signals has been accomplished. The results are proved to agree with the Heisenberg uncertainty relation. Furthermore, the theoretical results are verified by a Monte Carlo simulation, by using a signal generator and by experimental measurements with a laser Doppler velocimeter.

Two LSMs are applied for the QDT. (i) For the unweighted QDT it is shown that the minimum measuring error is reached for averaging times of approximately $1/\mathrm{e}$ and $1/\mathrm{e}^2$ signal duration, respectively, assuming dominating thermal and shot noise of the photo-electrical signal, respectively. Therefore, the signal processing has to consider these optimal averaging times in order to obtain good results. (ii) For the weighted QDT, using a defined weighting of the measurement values, the frequency measuring error is monotonically reduced towards the CRLB with increasing averaging time. In comparison with the unweighted QDT, a lower measuring error is reached, but the weighting has to be determined and the data rate of the centre-frequency calculation is lower. The unweighted QDT can be recommended for simple signal processing with good measuring accuracy, whereas the weighted QDT is the right choice for high precision measurements of frequency, e.g. of small velocity fluctuations in micro-turbulent flows.

This paper also communicates results on general aspects of the optimal processing of noisy single-tone Gaussian pulse signals. Viewed formally, Gaussian signals are not easy to handle, since they have theoretically an infinite signal duration. However, a suitable definition of the signal duration can be found in the context of the information content of the signal. Since the quality of the signal strongly decreases at the signal trailers, the main part of the information content lies in the centre of the signal. Using an unweighted QDT, an averaging time of approximately the full $1/\mathrm{e}^2$ signal duration Δt results in an optimal measuring result, assuming regime 1. Also the weighted QDT uses the main information content at the signal duration Δt, leading to a measuring error that exceeds the CRLB by only 15%, see section 7. Larger averaging times require greater efforts in memory and calculation for the LSM. Furthermore, they are limited due to the occurrence of the demodulation threshold. It can be argued that the full $1/\mathrm{e}^2$ duration can be viewed as the right choice for the evaluation of the signal time interval, assuming noise regime 1, i.e. the shot noise process.

It is stated that the statistical measuring error of the QDT is dependent only on the signal duration Δt and the SNR. In section 4.5, its independence of other parameters like the number of signal periods and sampling points has been shown. The result obtained is in agreement with the Heisenberg uncertainty relation. Therefore, frequency measurements at the fundamental limit of uncertainty can be accomplished by the QDT.

Acknowledgments

The author thanks O Dölle (LZH, now with Innolight, Hannover, Germany) for his professional support with Monte Carlo calculations. I am greatly indebted to my promoters Professor H Welling (LZH) and Professor F Hock (Universität Hannover, Germany). Furthermore, I want to thank Dr C Rathjen (CERN, Geneva, Switzerland) for support during the Maple programme, Dr H Müller (PTB, Braunschweig, Germany) and Dr P Regenfuß (LZH) for many motivating discussions. Last but not least, valuable advice from Dr H Nobach (Universität Darmstadt, Germany) and Dr H van Maanen (Shell, Amsterdam, The Netherlands) are acknowledged. This work was partially funded by the Deutsche Forschungsgemeinschaft (grant Cz55/7-1).

Appendix A. Linear regression

The standard deviation of the centre frequency of the burst signal is derived by means of the LSM. The sum of the least squares S of the differences between the straight regression line, equation (3), and the measured phase values has to be minimized. The partial derivatives of S (section 2) are set to zero:

$$\frac{\partial S}{\partial \hat{a}} = -2\sum_i (\phi_{Mi} - \hat{a} - \hat{b}t_i)w_i = 0.$$

$$\frac{\partial S}{\partial \hat{b}} = -2\sum_i (\phi_{Mi} - \hat{a} - \hat{b}t_i)t_i w_i = 0$$

The solution of the two equations results in

$$\hat{a} = \sum_i (\phi_{Mi} w_i) \Big/ \sum_i w_i - \hat{b}\Big(\sum_i (t_i w_i) \Big/ \sum_i w_i\Big)$$

$$\hat{b} = \Big(C\sum_i \phi_{Mi} w_i - \sum_i \phi_{Mi} t_i w_i\Big) \Big/ \Big(C\sum_i t_i w_i - \sum_i t_i^2 w_i\Big)$$

$$C = \Big(\sum_i t_i w_i\Big) \Big/ \sum_i w_i.$$

The factor C is zero for a symmetrical signal, see the Gaussian signal in equation (5). Otherwise it can be set to zero by a coordinate transformation. Then, the centre frequency of the signal is given by

$$\hat{f} = \frac{\hat{b}}{2\pi} = \frac{\sum_{i=-(N-1)/2}^{i=(N-1)/2} t_i \phi_{Mi} w_i}{2\pi \sum_{i=-(N-1)/2}^{i=(N-1)/2} t_i^2 w_i} \tag{A.1}$$

with N being an odd number of measurements. A similar formula can be derived for an even number of measurements.

Assuming an equal weight distribution, i.e. $w_i = 1$, $\forall i \in Z$, equation (A.1) can be simply written as

$$\hat{f} = \frac{\hat{b}}{2\pi} = \frac{\sum_{i=-(N-1)/2}^{i=(N-1)/2} t_i \phi_{Mi}}{2\pi \sum_{i=-(N-1)/2}^{i=(N-1)/2} t_i^2}. \tag{A.2}$$

Now, the standard deviation of the centre frequency will be derived. First, the measuring error of the weighted regression is considered on the basis of equation (A.1). According to the law of propagation of error the statistical measuring error of the phase values is given by

$$\Delta\hat{b} = \Bigg[\sum_{i=-(N-1)/2}^{i=(N-1)/2} \left(\frac{\partial(c_i\phi_{Mi})}{\partial\phi_{Mi}}\Delta\phi_{Mi}\right)^2\Bigg]^{1/2}$$

$$= \left(\sum_{i=-(N-1)/2}^{i=(N-1)/2} (c_i\Delta\phi_{Mi})^2\right)^{1/2}$$

$$c_i = \frac{t_i w_i}{\sum_{i=-(N-1)/2}^{i=(N-1)/2}(t_i^2 w_i)}$$

where c_i is a constant of the linear combination. Applying equation (4), the standard deviation of the centre frequency becomes

$$\Delta\hat{f} = \frac{\Delta\phi_{min}}{2\pi(\sum_{i=-(N-1)/2}^{i=(N-1)/2} t_i^2 w_i)^{1/2}} \tag{A.3}$$

where $\Delta\phi_{min}$ is the minimum standard deviation of the phase values of the time series, see section 4.4. The sampling times are assumed to be equidistant and can be written as

$$t_i = iT_S \qquad T_S = t_A/(N-1) \tag{A.4}$$

where T_S is the sampling period, given by the sampling frequency f_s as $T_S = 1/f_S$, t_A is the time duration of the time series and N is the odd number of measurements. Using equation (A.4), the denominator of equation (A.3) can be written as

$$\sum_{i=-(N-1)/2}^{i=(N-1)/2} t_i^2 w_i = \frac{t_A^2}{(N-1)^2} \sum_{i=-(N-1)/2}^{i=(N-1)/2} i^2 w_i$$

$$= \frac{2t_A^2}{(N-1)^2} \sum_{i=1}^{(N-1)/2} i^2 w_i. \tag{A.5}$$

For the right-hand side of this equation a symmetrical weighting function of the signal was assumed valid in order to simplify the calculation. Considering a Gaussian burst signal, this condition is fulfilled, see above. Applying these simplifications to equation (A.3) the standard deviation of the centre frequency is given by

$$\Delta\hat{f} = \frac{\Delta\hat{b}}{2\pi} = \frac{\Delta\phi_{min}}{(2^{3/2}\pi t_A/(N-1))(\sum_{i=1}^{(N-1)/2} i^2 w_i)^{1/2}}. \tag{A.6}$$

Next, the measuring error of an unweighted regression has to be derived. The estimation of the centre frequency is given by equation (A.2). However, the phase values of LDV signals generally have a different measuring error. In order to determine their centre frequency error, the weighting has to be considered. The measuring error is derived by analogy to the calculation of the weighted regression:

$$\Delta\hat{b} = \Bigg[\sum_{i=-(N-1)/2}^{i=(N-1)/2} \left(\frac{\partial(c_i\phi_{Mi})}{\partial\phi_{Mi}}\Delta\phi_{Mi}\right)^2\Bigg]^{1/2}$$

$$= \left(\sum_{i=-(N-1)/2}^{i=(N-1)/2} (c_i\Delta\phi_{Mi})^2\right)^{1/2}$$

$$c_i = \frac{t_i}{\sum_{i=-(N-1)/2}^{i=(N-1)/2} t_i^2}.$$

Applying equations (4) and (A.4) the standard deviation of the centre frequency is given by

$$\Delta\hat{f} = \frac{\Delta\hat{b}}{2\pi} = \frac{\Delta\phi_{min}(\sum_{i=-(N-1)/2}^{(N-1)/2} t_i^2/w_i)^{1/2}}{2\pi \sum_{i=-(N-1)/2}^{(N-1)/2} t_i^2}.$$

Using equation (A.5), the standard deviation turns out to be

$$\Delta\hat{f} = \frac{\Delta\hat{b}}{2\pi} = \frac{\Delta\phi_{min}(\sum_{i=1}^{(N-1)/2} i^2/w_i)^{1/2}}{(2^{3/2}\pi t_A/(N-1)) \sum_{i=1}^{(N-1)/2} t_i^2}. \qquad (A.7)$$

The presumption of a symmetrical weighting w_i of the time series and an odd number of phase values N does not affect the universal validity.

Appendix B: The Heisenberg uncertainty relation

The uncertainty relation between the position x and the momentum p as canonic, conjugated variables was formulated by Heisenberg in 1927: $\Delta x \Delta p \geqslant h/(4\pi)$, where Δx and Δp are the standard deviations of the expectation values of position and momentum and h is Planck's quantum. A Gaussian distribution of both variables gives the minimum values $h/(4\pi)$ of the inequality. For an optical wave pulse propagating along the x-axis, the substitution $x = ct$ can be made, where c is the velocity of light and t is the retardation time. The momentum can be written as $p = hf/c$, where f is the frequency of the optical wave or also of an electrical signal. Then the Heisenberg uncertainty relation can be formulated as

$$\Delta t \Delta f \geqslant 1/(4\pi) \qquad (B.1)$$

where the variances are defined as $(\Delta t)^2 = \int t^2[A(t)]^2\,\mathrm{d}t / \int [A(t)]^2\,\mathrm{d}t$ and $(\Delta f)^2 = \int f^2[A'(f)]^2\,\mathrm{d}t / \int [A'(f)]^2\,\mathrm{d}f$ with $A(t) = A_0 \exp[-(t/\tau)^2]$ and $A'(f)$ as its Fourier transformation. The standard deviation of the time-dependent function can be interpreted as the half 1/e duration of the Gaussian pulse signal. Spectral broadening of the wave corresponds to the standard deviation of the frequency. The measuring error of the centre frequency $\Delta\hat{f}$ is proportional to the signal line width Δf.

The optical wave can be considered as a photon ensemble in terms of quantum mechanics. Then the momentum can be written as $p = E/c$, where E is the energy of the photon ensemble. The standard deviation turns out to be $\Delta p = \Delta E/c = \Delta n h f/c$, where n is the number of photons and hf is the single photon energy. The phase ϕ of the wave is given by $\phi = 2\pi f t$ and its standard deviation can be written as $\Delta\phi = 2\pi f \Delta t = 2\pi f \Delta x/c$, where the relation $x = ct$ is used, see above. Then the Heisenberg uncertainty relation reads [9]

$$\Delta\phi \Delta n \geqslant \tfrac{1}{2}. \qquad (B.2)$$

The standard deviation of the number of photons can be investigated with photon statistics. A coherent laser beam exhibits a Poisson distribution of the number of photons: $p(n) = \langle n\rangle^n[\exp(-\langle n\rangle)]/n!$. This expression describes the quantum noise of the photon ensemble. It is equal to the shot noise of the electron current for an ideal photo-detector with 100% quantum efficiency.

It is pointed out that a lower phase variance than that for shot noise processes can be achieved by using so-called squeezed light, causing e.g. anti-bunching of the photons. Its variance is reduced, however, only at certain phase angles of the sinusoidal signal. Furthermore, squeezed light is usually suppressed by dissipation processes, which occur e.g. during the scattering of light in LDV systems.

The SNR of coherent light is assumed to be SNR $= \langle n\rangle/\Delta n = \langle n\rangle^{1/2}$, so equation (B.2) can be written as $\Delta\phi \geqslant 1/(2\langle n\rangle^{1/2}) \sim \mathrm{SNR}^{-1/2}$. Using the proportionality of the average optical power to the number of photons $P \sim \langle n\rangle$ results in $\Delta\phi \sim P^{-1/2} \sim A^{-1/2}$. This result is equal to equation (12), which was derived for the phase measurement of a signal with superposed shot noise, see section 4.2. Together with equation (18) the proportionality $\Delta\hat{f} \sim \Delta\phi \sim P^{-1/2}$ is obtained, with $\Delta\phi_{min}$ set to $\Delta\phi$. In conclusion, the optical power is a fundamental parameter of the frequency measuring error.

References

[1] Shinpaugh K, Simpson R, Wicks A, Ha S and Fleming J 1992 Signal-processing techniques for low signal-to-noise ratio laser Doppler velocimetry signals *Exp. Fluids* **12** 319–28

[2] van Maanen H R E 1999 Retrieval of turbulence and turbulence properties from randomly sampled laser-Doppler anemometry data with noise *PhD Thesis* TU-Delft

[3] Strunck V, Müller H and Dopheide D 1996 Time domain single-tone analysis using quadrature algorithm *Proc. 8th Int. Symp. on Applications of Laser Techniques to Fluid Mechanics (Lisbon)* paper 6.6

[4] Czarske J and Dölle O 1998 Quadrature demodulation technique used in laser Doppler anemometry *Electron. Lett.* **43** 547–9

[5] Czarske J, Hock F and Müller H 1993 Quadrature demodulation—a new LDV-burst signal frequency estimator *Proc. 5th Int. Conf. on Laser Anemometry—Advances and Applications (Veldhoven, 23–27 August 1993)* ed J Bessem *et al* (Bellingham, WA: SPIE)

[6] Müller H, Strunck V and Dopheide D 1996 The application of quadrature demodulation techniques for the investigation of flows *Flow Meas. Instrum.* **7** 237–45

[7] Czarske J 1996 Method for analysis of the fundamental measuring uncertainty of laser Doppler velocimeters *Opt. Lett.* **21** 522–4

[8] Minkoff J 1992 *Signals, Noise and Active Sensors—Radar, Sonar and Laser Radar* (New York: Wiley)

[9] Pedrotti L, Sanders V and Scully M 1984 On the number-phase uncertainty relationship for a laser *Proc. SPIE* **487** ed S Jacobs *et al* 39–41

[10] Rife D and Boorstyn R 1974 Single-tone parameter estimation from discrete-time observations *IEEE Trans. Information Theory* **20** 591–8

[11] Boashash B, O'Shea P and Arnold M 1990 Algorithms for instantaneous frequency estimation: a comparative study *Proc. SPIE* **1348** ed F Luk 126–48

[12] Lading L and Andersen K 1990 Estimating frequency and phase for velocity and size measurements *Laser Anemometry* ed J T Turner (Oxford: Springer) pp 161–8

[13] Matovic D and Tropea C 1991 Spectral peak interpolation with application to LDA signal processing *Meas. Sci. Technol.* **2** 1100–6

[14] Lehmann P 1998 Determination of Doppler frequencies and characteristic frequency modulation phenomena in laser Doppler signals *Proc. 9th Int. Symp. on Applications of Laser Techniques to Fluid Mechanics (Lisbon, 13–16 July)* ed R Adrian *et al* paper 32.3

[15] Lehmann B and Helbig J 2000 Local acquisition of mean and turbulent fluid acceleration in highly turbulent flow by the means of laser-Doppler velocimetry *10th Int. Symp.—Applications of Laser Techniques to Fluid Mechanics (Lisbon, 10–13 July)* ed R Adrian *et al* paper 17.2
[16] Nobach H 1999 Advanced techniques for frequency estimation from LDA burst signals *Proc. 8th Int. Conf. on Laser Anemometry—Advances and Applications (Rome, 6–8 September)* pp 311–8
[17] Nobach H 2000 Verarbeitung von LDA-Signalen beschleunigter Streuteilchen *8th Conf. on Lasermethoden in der Strömungsmeßtechnik (Freising/Weihenstephan, 12–14 September)* paper 7
[18] Schultheiss P, Wogrin C and Zweig F 1954 Short-time frequency measurement of narrow-band random signals in the presence of wide-band noise *J. Appl. Phys.* **25** 1025–36
[19] Steinberg H, Schultheiss P, Wogrin C and Zweig F 1955 Short-time frequency measurement of narrow-band random signals by means of a zero counting process *J. Appl. Phys.* **26** 195–201
[20] Adrian R J 1972 Statistics of laser Dopper velocimeter signals: frequency measurement *J. Phys. E: Sci. Instrum.* **5** 91–5
[21] Adrian R J, Humphrey J and Whitelaw J 1975 Frequency measurement error due to noise *Proc. LDA-Symp. 75 (Copenhagen)* (Skovlunde: Dantec Measurement Technology) pp 287–99
[22] George W K 1975 Limitations to measuring accuracy inherent in the laser Doppler signal *Proc. LDA-Symp. 75 (Copenhagen)* pp 20–63 [reprinted in selected papers on laser Doppler velocimetry, SPIE Milestone Series 78 ed R J Adrian (Bellingham, WA, SPIE) pp 135–64]
[23] Hoesel W and Rodi W 1975 Errors occurring in LDA-measurements *Proc. LDA-Symp. 75 (Copenhagen)* pp 251–61
[24] McWirter J G and Pike ER 1979 The extraction of information from laser anemometry data *Phys. Scr.* **19** 417–25
[25] Drain L 1980 *The Laser Doppler Technique* (Chichester: Wiley)
[26] Ruck B and Pavlovski B 1995 Grenze der Genauigkeit in der Zeitbereichsauswertung der Laser-Doppler-Anemometrie *Techn. Messen* **62** 292–8
Ruck B and Pavlovski B 1995 Grenze der Genauigkeit bei der LDA-Turbulenzmessung *4th Conf. on Lasermethoden in der Strömungsmeßtechnik (Rostock, 12–14 September)* paper 5
Ruck B and Pavlovski B 1996 Digitalisierungsfehler durch Amplitudenquantisierung bei der Auswertung von LDA-Signalen *5th Conf. on Lasermethoden in der Strömungsmeßtechnik (Berlin, 11–13 September)* paper 8
Ruck B and Pavlovski B 1999 Auswertung von LDA-Signalen im Zeitbereich bei geringer Turbulenz *7th Conf. on Lasermethoden in der Strömungsmeßtechnik (Saint-Louis, 27–29 September)* paper 3
[27] Czarske J, Zellmer H and Welling H 1999 Directional achromatic heterodyne fiber laser Doppler anemometer *Opt. Commun.* **132** 421–6
[28] Eadie W, Dryard D, James F, Roos M and Sadoulet B 1988 *Statistical Methods in Experimental Physics* (Amsterdam: North-Holland)
[29] Jones J J 1967 *Modern Communication Principles* (New York: McGraw Hill)
[30] Lading L and Jorgensen T M 1990 Maximizing the information transfer in a quantum-limited light scattering system *J. Opt. Soc. Am.* A **7** 1324–31
[31] Boashash B 1992 Estimating and interpreting the instantaneous frequency of a signal—part 2: algorithms and applications *Proc. IEEE* **80** 540–68
[32] Czarske J 1996 *Verfahren zur Messung und Auswertung der Interferenzphase in der Laser-Doppler-Velocimetrie* (Düsseldorf: VDI) Report vol. 8, no 530
[33] Oppenheim A and Schäfer R 1989 *Discrete-Time Signal Processing* (Englewood Cliffs, NJ: Prentice Hall)
[34] Rathjen C 1995 Statistical properties of phase-shift algorithms *J. Opt. Soc. Am.* A **12** 1997–2008
[35] Kozdon A 1991 *Practical Aspects of a Least-Squares Regression for Polynomials* (Braunschweig: PTB) Report W44
[36] Cecchi G 1991 Error analysis of the parameters of a least-squares determined curve when both variables have uncertainties *Meas. Sci. Technol.* **2** 1127–8
[37] Skolnik M I 1980 *Introduction to Radar Systems* (New York: McGraw-Hill) ch 11
[38] Ibrahim K and Bachalo W 1996 A novel architecture for real-time phase measurement *Proc. 8th Int. Symp. on Applications of Laser Techniques to Fluid Mechanics (Lisbon, 8–11 July)* ed R Adrian *et al* paper 2.3
[39] Tropea C 1995 Laser Doppler anemometry: recent developments and future challenges *Meas. Sci. Technol.* **6** 605–19
[40] Benedict L, Nobach H and Tropea C 2000 Estimation of turbulent velocity spectra from laser Doppler data *Meas. Sci. Technol.* **11** 1089–104